INFORMATION TO USERS

This reproduction was made from a copy of a document sent to us for microfilming. While the most advanced technology has been used to photograph and reproduce this document, the quality of the reproduction is heavily dependent upon the quality of the material submitted.

The following explanation of techniques is provided to help clarify markings or notations which may appear on this reproduction.

1. The sign or "target" for pages apparently lacking from the document photographed is "Missing Page(s)". If it was possible to obtain the missing page(s) or section, they are spliced into the film along with adjacent pages. This may have necessitated cutting through an image and duplicating adjacent pages to assure complete continuity.

2. When an image on the film is obliterated with a round black mark, it is an indication of either blurred copy because of movement during exposure, duplicate copy, or copyrighted materials that should not have been filmed. For blurred pages, a good image of the page can be found in the adjacent frame. If copyrighted materials were deleted, a target note will appear listing the pages in the adjacent frame.

3. When a map, drawing or chart, etc., is part of the material being photographed, a definite method of "sectioning" the material has been followed. It is customary to begin filming at the upper left hand corner of a large sheet and to continue from left to right in equal sections with small overlaps. If necessary, sectioning is continued again—beginning below the first row and continuing on until complete.

4. For illustrations that cannot be satisfactorily reproduced by xerographic means, photographic prints can be purchased at additional cost and inserted into your xerographic copy. These prints are available upon request from the Dissertations Customer Services Department.

5. Some pages in any document may have indistinct print. In all cases the best available copy has been filmed.

University Microfilms International
300 N. Zeeb Road
Ann Arbor, MI 48106

Order Number 1331474

Thermally evaporated bistable thin film etalons

Sprague, Robert Wendell, M.S.

The University of Arizona, 1987

THERMALLY EVAPORATED BISTABLE THIN FILM ETALONS

by

Robert Wendell Sprague

A Thesis Submitted to the

COMMITTEE ON OPTICAL SCIENCES (GRADUATE)

In Partial Fulfillment of the Requirements
For the Degree of

MASTER OF SCIENCE

In the Graduate College

THE UNIVERSITY OF ARIZONA

1 9 8 7

STATEMENT BY AUTHOR

This thesis has been submitted in partial fulfillment of requirements for an advanced degree at The University of Arizona and is deposited in the University of Arizona and is deposited in the University Library to be made available to borrowers under rules of the Library.

Brief quotations from this thesis are allowable without special permission, provided that accurate acknowledgment of source is made. Requests for permission for extended quotation from or reproduction of this manuscript in whole or in part may be granted by the head of the major department or the Dean of the Graduate College when in his or her judgment the proposed use of the material is in the interests of scholarship. In all other instances, however, permission must be obtained from the author.

SIGNED: Robert W Sprague

APPROVAL BY THESIS DIRECTOR

This thesis has been approved on the date shown below:

H. G. Macleod
H. ANGUS MACLEOD
Professor of Optical Sciences

30 June 1987
Date

Tempis Fugit

Preface

Thin-film narrow band filters, long a mainstay of the optical coating industry, have recently been shown to exhibit bistability. The projected applications of these devices are manifold and of great interest. Many predictions as to their optimum performance have been made. In this thesis we have investigated the experimentally obtainable performance and measured the switching characteristics of Zinc sulfide (ZnS)-Chiolite interference filters dependence on the spacer thickness and reflectivity of the mirrors.

I would like to take this opportunity to to thank all the people who have contributed to this endeavor, many of whom will go unnamed but whose influence has been and continues to be important.

First I must thank my parents "without whom none of this would have been possible".

I wish to thank: H. Angus Macleod for his support and patience over the past 5 years; Ross Potoff for his insight into all things mechanical and for imparting at least a small portion of it to me; Bertrand Bovard for his very careful reading of the manuscript as well as many helpful discussions along the way; Ursula Gibson for her friendship and assistance in my final exam; and the following friends who convinced me that an advanced degree would be of benefit: Glenn Boreman, Terry Fergusson, Chris Karaguleff, Jack Jewell, and Russell Chipman.

Finally I would like to acknowledge: The Optical Circuits Cooperative for their funding support; and the following coworkers without whose time and dedication none of these measurements would have been possible: H.M. Chou, M.T. Tsoa, L. Wang, R. Jin, and G. Gigioli.

TABLE OF CONTENTS

TABLE OF CONTENTS (Continued)

List of Illustrations

List of Illustrations (Continued)

Abstract

Passive intrinsic bistability is of great interest. Our Fabry-Perot interference filters exhibit bistability due to a temperature dependent refractive index. Operating across the entire viable spectrum permits wide application to the demonstration and development of concepts for optical computing.

Thermal evaporation of zinc sulfide and chiolite is used to produce Fabry-Perot interference filters. The effect of the thickness of the spacer, and reflectivities of the mirrors, on the nonlinear characteristics of these devices is investigated.

The mathematic description of these etalons linear, as well as their nonlinear, behavior is presented. The experimental apparatus is described. Measured values of the minimum critical detuning and minimum observed power are presented.

INTRODUCTION

Optical bistability and the associated nonlinearity observed in optical materials are of interest to a growing number of people in the optics community. This interest is, in part, generated by possible applications of these effects. In particular a large number of researchers are interested in the question "What can optics do for computing? " (Lohman, 1986). Electronic digital computing is approaching the limits imposed by the Von Neuman architectures, particularly by the problem of communication (Huang, 1983). Devices such as optical memories and transistors for applications to optical signal processing and computing are envisioned. These devices would exploit the inherent two dimensionality of imaging systems to circumvent the "bottleneck" associated with serial communication.

Light waves propagating in a linear medium do not interact. This non-interaction of photons is simultaneously the boon and bane of optical computing. It eases communications constraints, while complicating logic. To do logical operations with light entails the introduction of nonlinear phenomena. Nonlinear phenomena imply materials that have some property, such as refractive index, which is a function of the irradience level.

In Fabry-Perot narrow band interference filters multiple beam interference creates an amplification of the electric field in the cavity. If constructed with a nonlinear medium in the spacer layer and illuminated with a monochromatic source they can be tuned to perform logical AND (transmission) or NAND

(reflection) on a large number of independent spots (Olbright et al, 1984). These filters, constructed with a spacer of zinc sulfide, exhibit a hysteresis loop as a function of incident irradiance. Figure 1.1 is a loop obtained in this work. Bistability results from the temperature dependent refractive index of the ZnS. The absorption inherent in the films causes the filter to heat up, increases the phase thickness of the spacer, and shifts the peak transmittance wavelength of the filter. The filter thus switches from a low to a high transmittance, i.e. between off and on.

In this thesis I discuss the effects of some design parameters available to the thin film worker which affect the switching characteristics of Fabry-Perot narrow band filters. We have varied the phase thickness of the spacer while attempting to maintain the reflectivity of the endmirrors. We have also varied the the reflectivities of the mirror for certain spacer thicknesses.

The thesis is arranged as follows. The theory of the linear Fabry-Perot filter is presented from the basic mathematics. Bistability is then discussed in the context of a thermal refractive mechanism. The means of producing the filters and the subsequent performance are outlined. Finally the results of the experiment are discussed. I have attempted to use consistent notation through out. Boldface is used for vector quantities, script for the corresponding magnitudes.

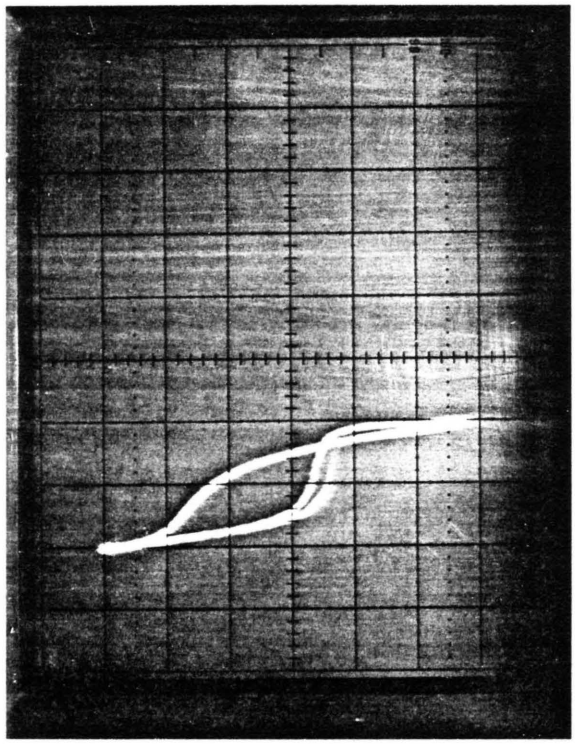

Figure 1.1 *Bistable loop of an early ZnS etalon*

LINEAR ASPECTS OF FABRY PEROT FILTERS

The linear aspects of Fabry-Perot narrow band interference filters (NBF) are well understood (Born and Wolf, 1980). They are essentially Fabry Perot etalons (1899) with an effective plate separation which is determined by the optical thickness of the center layer. The necessary mathematics for their quantitative description is presented here.

These phenomena are classically described by Maxwell's equations, which are reduced in complexity through the assumption of a homogeneous linear isotropic medium. Nevertheless it should be noted that this simple case is extendable: an inhomogeneous medium can be modeled as a composite of homogeneous parts; an anisotropic medium can, in the important cases of propagation along the principle axes, be generalized from an isotropic one through the polarizability of the medium.

The format of this discussion is as follows. Starting with Maxwell's equations, the traveling plane wave solution in an infinite medium is obtained. This solution is then applied to a single boundary, and the Fresnel equations for the amplitude reflection and transmission coefficients are derived. By introducing a second interface, one extracts the interference condition for a layer of finite thickness. This single layer is then generalized to the case of an arbitrary multilayer. The Fabry-Perot NBF is then presented as a special case of a general multilayer.

MAXWELL'S EQUATIONS

These phenomenological equations describing the macroscopic behavior of the interaction of light and matter can be written in S.I. units as:

$$\nabla \times \mathbf{B} = \mu \mathbf{j} + \frac{\mu \partial \mathbf{D}}{\partial t} \qquad 2.1$$

$$\nabla \times \mathbf{E} = -\frac{\partial \mathbf{B}}{\partial t} \qquad 2.2$$

$$\nabla \cdot \mathbf{D} = \rho \qquad 2.3$$

$$\nabla \cdot \mathbf{B} = 0 \qquad 2.4$$

Where: $\mathbf{B} = \mu_0(\mathbf{H} + \mathbf{M}) = \mu \mathbf{H}$, is the magnetic field;

$\mathbf{D} = \epsilon_0 \mathbf{E} + \mathbf{P} = \epsilon \mathbf{E}$ is the Displacement;

$\mathbf{j} = \sigma \mathbf{E}$ the current density.

In the visible region of the electromagnetic spectrum dielectric materials can be treated as though the magnetization, M, and the free charge density, ρ, are identically zero without any loss of applicability. The assumption that these dielectric materials are lossless is not made.

The Wave Equation

With the restriction mentioned above the wave equation is obtained by taking the curl of equation 2.2,

$$\nabla x \nabla x E = \nabla \times \left[-\frac{\partial B}{\partial t} \right]. \qquad 2.6$$

A vector identity for the triple product is then applied to equation 2.6 resulting in;

$$\nabla(\nabla \cdot E) - \nabla^2 E = -\frac{\partial}{\partial t}(\nabla x B). \qquad 2.7$$

The first term in equation 2.7 is zero, and the last term is replaced using eqn.(2.1), to obtain :

$$-\nabla^2 E = -\frac{\partial}{\partial t}\left[\mu \left[j + \frac{\partial D}{\partial t} \right] \right] . \qquad 2.8$$

This is rearranged to yield:

$$\nabla^2 E = \mu\sigma \frac{\partial E}{\partial t} + \mu\epsilon \frac{\partial^2 E}{\partial^2 t} \qquad 2.9$$

or

$$\nabla^2 E - \mu\sigma \frac{\partial E}{\partial t} - \mu\epsilon \frac{\partial^2 E}{\partial^2 t} = 0 . \qquad 2.10$$

This linear second order differential equation is referred to as the wave equation. It is the electric field which is of prime concern in this treatment of matter-light interactions, but a similar argument can be made for the magnetic field, H, resulting in an analogous equation.

The wave equation is known to have travelling plane wave solutions, of the form:

$$E = E_0 e^{\left\{ i\omega \left[t - \frac{r}{v} \right] \right\}} . \qquad 2.11$$

Here: r is the position vector; ω is the frequency, $2\pi/\lambda$; λ is the wavelength; v is the velocity; and E_0 is the amplitude, including direction of polarization. Equation 2.11 is a solution to equation 2.10 if and only if

$$\frac{1}{v^2} = \epsilon\mu - \frac{i4\pi\sigma\mu}{\omega} . \qquad 2.12$$

The velocity, v, of the traveling wave is a complex quantity. Identifying the susceptibilities $\epsilon=\epsilon_r\epsilon_0$ and $\mu=\mu_r\mu_0$, as linear scalar quantities with relative permittivity ϵ_r and permeability μ_r, the complex refractive index, N, is defined as:

$$N^2 \equiv \frac{c^2}{v^2} = \epsilon_r\mu_r - i4\pi\mu_r\frac{\sigma}{\omega} . \qquad 2.13$$

Where the relation $c^2\epsilon_0\mu_0=1$ is used. If we now choose N to have the form n-ik, and set $\mu_r = 1$ at optical frequencies, then the fundamental properties of the material are related to the optical constants by

$$nk = \frac{2\pi\sigma}{\omega} \qquad 2.14$$

and

$$n^2 - k^2 = \epsilon \qquad 2.15$$

A further material parameter of interest is the optical admittance of a material, Y. The admittance of a wave propagating in an infinite medium is defined as the ratio of magnetic to electric field magnitudes $\mathcal{H}/\mathcal{E}$. In the absence of free space charge, ρ, and magnetization, M, the refractive index and the optical admittance are linearly related by

$$Y=Y_0N. \qquad 2.16$$

The admittance of free space, Y_0 is equal to 1/377 siemens.

Often it is ratios of quantities, not their absolute magnitudes, that are of interest. In these cases one normalizes admittances to "free space units", by setting the admittance numerically equal to the refractive index.

A travelling plane wave, in a cartesian system of coordinates (x,y,z), with direction cosines (α,β,γ), and free space wavelength λ, in medium of refractive index N, is of the form:

$$E=E_0\, e^{\left\{i\left[\omega t-\frac{2\pi N}{\lambda}\,[\alpha x+\beta y+\gamma z]\right]\right\}}$$

$$=E_0\, e^{\left\{i\left[\omega t-\frac{2\pi}{\lambda}\,(n-ik)[\alpha x+\beta y+\gamma z]\right]\right\}}$$

$$=E_0\, e^{\left\{-\frac{2\pi k}{\lambda}\,(\alpha x+\beta y+\gamma z)\right\}}\; e^{\left\{i\left[\omega t-\frac{2\pi n}{\lambda}\,(\alpha x+\beta y+\gamma z)\right]\right\}} \qquad 2.17$$

With these choices of form for the travelling wave and refractive index, the imaginary portion of the complex dielectric constant is identified with an attenuation of the field. The real part of the refractive index is associated with phase change and propagation of the field.

SINGLE INTERFACE

Thin film optics is intrinsically the study of interfaces between different media. At an interface, the discontinuity in the optical properties results in the

reflection of a portion of the incident flux. In the linear regime the ratios of the incident, reflected and transmitted fields, and irradiances, are independent of the incident magnitude. We define the amplitude reflection coefficient, ρ (regrettably the same symbol as the free space charge above), and amplitude transmittance coefficient, τ, as the ratio of the reflected, or transmitted, field to incident field. Inclusion of residual loss, through absorption or scatter, at the interface complicates the problem but makes it more realistic.

Any arbitrary polarization of an electromagnetic wave can be decomposed into a linear combination of two orthogonal basis states (Hecht and Zajac, 1974). The following analysis uses linear polarization states for the basis, chosen to reflect the inherent symmetry of the model. The two states are conventionally referred to as the **S** and **P** polarizations. **S** polarized light is defined as having the electric field vector normal to the plane of incidence (parallel to the interface of the two materials). Electromagnetic radiation of the **P** polarization has the electric field in the plane of incidence. The plane of incidence is defined by the propagation vector and the normal to the surface.

At this point it is necessary to choose sign conventions. In this work the sign convention will be established through the following considerations, as illustrated in figure 2.1.

The electric field, magnetic field and propagation vectors comprise a right handed set. Once the direction of propagation and one of the fields are established then the third quantity of interest is determined. The sign conventions are chosen such that the **P** polarized component of the electric field (which is of greater interest to us than the magnetic) retains the same sign in the incident and reflected beams for normal and nonnormal incidence.

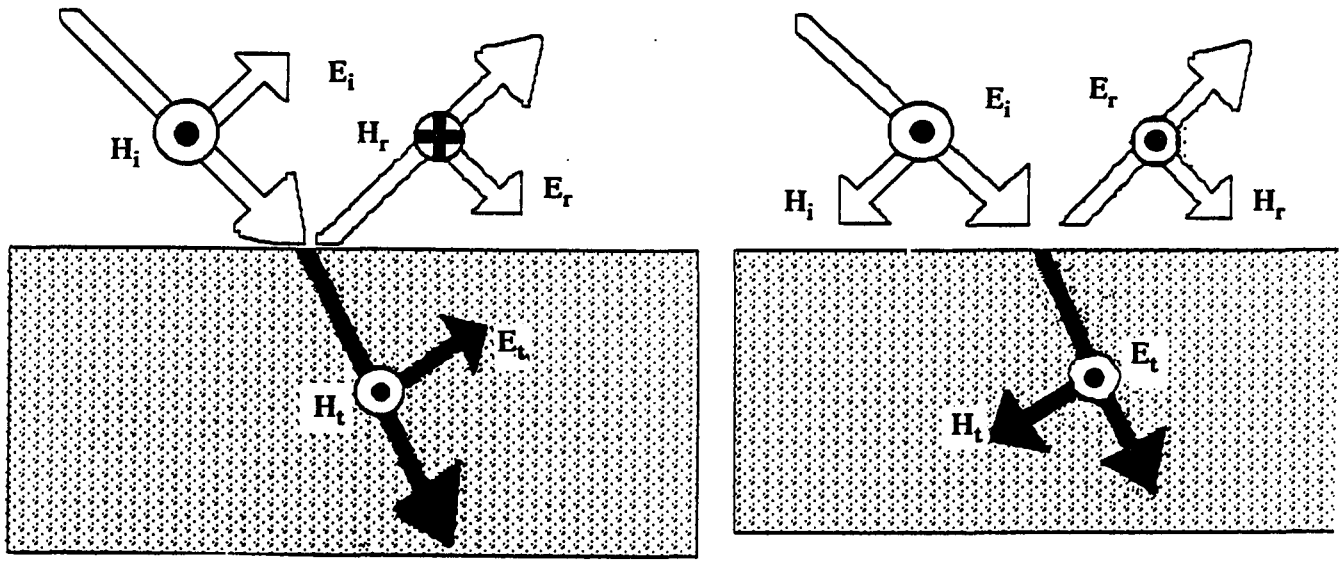

S Polarized **P Polarized**

E_i the incident electric field
E_r the reflected electric field
E_t the transmitted electric field
θ_i the incident angle
$\alpha_r, \beta_r, \gamma_r$ the reflected direction cosines
$\alpha_t, \beta_t, \gamma_t$ the transmitted direction cosines

Figure 2.1 *Light Incident On An Interface*

In general the boundary conditions at an interface are satisfied if one assumes that an incident wave is split into transmitted and reflected portions (Macleod, 1986).

Let

$$E_i = E_i e^{\left\{ i\left[\omega t - \left[\frac{2\pi N_1}{\lambda} \right] (x\sin\theta_1 + y\cos\theta_1) \right] \right\}} \qquad 2.18$$

$$E_r = E_r e^{\left\{ i\left[\omega t - \left[\frac{2\pi N_1}{\lambda} \right] (\alpha_r x + \beta_r y + \gamma_r z) + \delta_r \right] \right\}} \qquad 2.19$$

$$E_t = E_t e^{\left\{ i\left[\omega t - \left[\frac{2\pi N_2}{\lambda} \right] (\alpha_t x + B_t y + \gamma_t z) + \delta_t \right] \right\}} \qquad 2.20$$

be the general solution consisting of an incident, E_i, a reflected, E_r, and a transmitted E_t wave field.

Applying the boundary conditions, i.e. the tangential component of E and H are continuous across the interface independent of location and time then:

(i) $\delta_r = \delta_t = 0$

(ii) $\omega_i = \omega_r = \omega_t = \omega$

(iii) $N_1\beta_r = N_2\beta_t = 0$

(iv) $N_1\sin\theta_1 = N_1\alpha_r = N_2\alpha_t$. 2.21

(i) and (ii) state that the incident and reflected wave have the same wavelength and phase; (iii) and (iv) imply Snell's law obtains in vector form.

These relations are valid whether N is real or complex. In the complex case it should be noted that the planes of constant phase are no longer parallel to the planes of constant amplitude. The planes of constant phase are perpendicular to the oblique direction of propagation and the planes of constant amplitude are parallel to the interface.

The two linear polarizations are considered independently.

S Polarization

For the case of a travelling wave with the electric field perpendicular to the plane of incidence, the continuity of the tangential components of the electric and magnetic fields across the interface yields the equations:

$$-H_i\cos\theta_i+H_r\cos\theta_r = -H_t\cos\theta_t \qquad 2.22$$

$$E_i+E_r=E_t \qquad 2.23$$

or

$$\frac{1}{\mu_i v_i}(E_i-E_r)\cos\theta_i = \frac{1}{\mu_t v_t}E_t\cos\theta_t \qquad 2.24$$

$$\frac{N_i}{\mu_i}(E_i-E_r)\cos\theta_i = \frac{N_t}{\mu_t}E_t\cos\theta_t \qquad 2.25$$

and solving for the amplitude reflection and transmittance coefficients while setting

the relative magnetic permeability equal to one.

$$\rho_s = \frac{N_i\cos\theta_i - N_t\cos\theta_t}{N_i\cos\theta_i + N_t\cos\theta_t} \qquad 2.26$$

$$\tau_s = \frac{2N_i\cos\theta_i}{N_t\cos\theta_t + N_i\cos\theta_i} \qquad 2.27$$

P Polarization

For the case of P polarized light the boundary conditions lead to :

$$E_i\cos\theta_i + E_r\cos\theta_r = E_t\cos\theta_t \qquad 2.28$$

$$\frac{E_i}{\mu_i}v_i - \frac{E_r}{\mu_i}v_i = \frac{E_t}{\mu_t}v_t \qquad 2.29$$

and the Fresnel coefficients (with $\mu_i = \mu_t = 1$) become;

$$\tau_p = \frac{2N_i\cos\theta_i}{N_t\cos\theta_i + N_i\cos\theta_t}. \qquad 2.30$$

$$\rho_p = \frac{N_i\cos\theta_t - N_t\cos\theta_i}{N_i\cos\theta_i + N_t\cos\theta_t}. \qquad 2.31$$

These are the total reflected and transmitted waves. In thin film work, where one is usually interested in energy transmitted through a structure, it is customary to work with the component of the electric field parallel with the interface, not the total fields. To this end eq. 2.30 needs to be modified. Define τ_p(parallel) as

$$\tau_p(\text{parallel}) = (E_t\cos\theta_t)/(E_i\cos\theta_i) \qquad 2.32$$

whereby 2.36 is obtained

$$\tau_p = \frac{2N_i \cos\theta_t}{N_t \cos\theta_i + N_i \cos\theta_t} . \qquad 2.33$$

Unless otherwise noted, any further reference to τ_p shall be to τ_p(parallel).

One can simplify the form of the Fresnel coefficients through the inclusion of polarization effects in the optical admittance. The effective admittances η_p for P polarized light, and η_s for the S polarization are defined from the the components of E and H parallel to the boundary as

$$\eta_p = Y_0 N/\cos\theta \qquad 2.34$$

$$\eta_s = Y_0 N\cos\theta . \qquad 2.35$$

Y_0 is the admittance of free space.

The amplitude reflection and transmission coefficients then become :

$$\rho = \frac{\eta_i - \eta_t}{\eta_i + \eta_t} \qquad 2.36$$

$$\tau = \frac{2\eta_i}{\eta_i + \eta_t} . \qquad 2.37$$

We note that at a single ideal interface there can be no absorption. Although these coefficients, τ and ρ, are the fundamental coefficients governing the properties of the interface, it is the time averaged Poynting vector that determines measurable quantities.

A THIN FILM

The Fresnel coefficients derived above apply to any interface. To predict the behavior of a real sample the effects of a second interface must be considered.

For a thick medium, no definite phase relation exists between the field incident on the medium and that which is reflected from the back surface. The material is thicker than the coherence length of the source, and consequently each surface is treated independently. The observables, reflectance or transmittance, of a thick medium are obtained by addition of the squared modulus of the field.

For a thin film, where fields at the front and back surfaces have a finite phase relation both interfaces must be considered in determining the behavior. This occurs whenever the optical path length (opl) for a round trip in the material is less than the coherence length of the source.

The 'thinness' of a film is a function of the source of illumination as much as the film's physical dimensions. The behavior of a thin film can be calculated using two equivalent methods, geometric and electromagnetic.

In the geometric approach the reflected field is found by summing over all rays at the first surface of the film. Figure 2.2 indicates the quantities of interest for a thin film between two semi-infinite media. The admittances of the three media are Y_0, Y_1, Y_2, with refractive indices N_0, N_1, N_2 . The thin film has a physical thickness d and a phase thickness $\delta=2\pi N_1 d\cos\theta/\lambda$. The interfaces have reflection and transmission coefficients ρ_{a^+}, ρ_{a^-}, τ_{a^+}, τ_{a^-}, ρ_{b^+}, ρ_{b^-}, τ_{b^+}, τ_{b^-} ; the $\mp$, indicate the direction of propagation, and the subscripts (a,b) specify

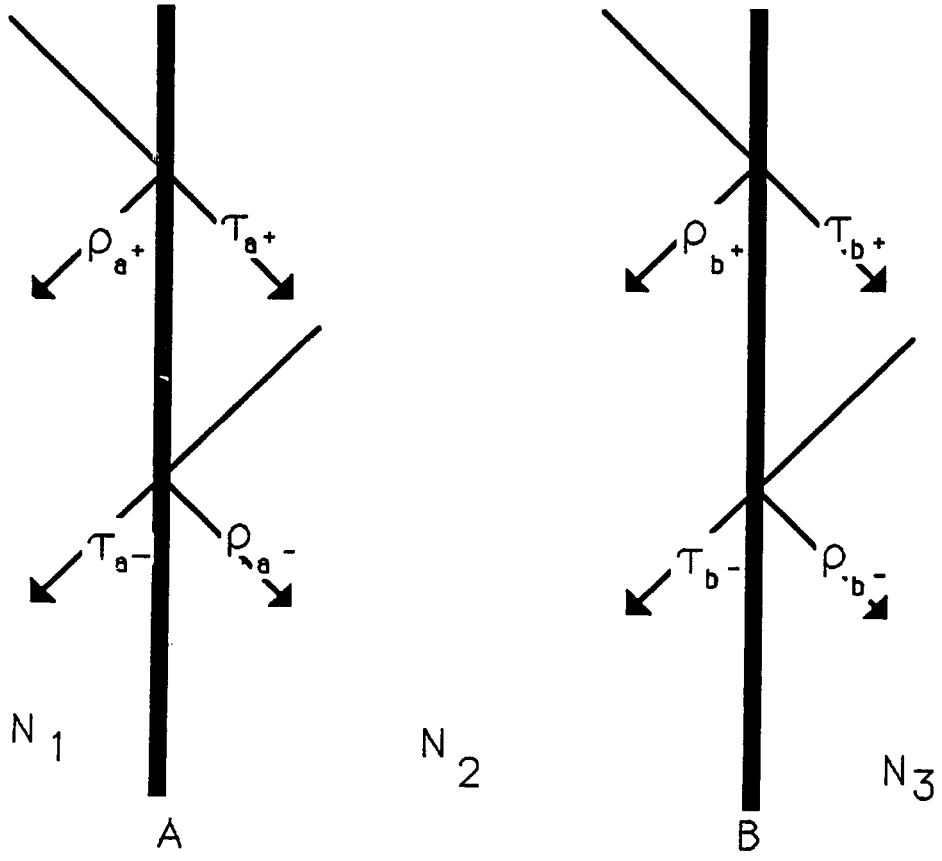

τ_{a^+}	Forward Transmittance at A interface, from 1 to 2
τ_{a^-}	Reverse Transmittance at A interface, from 2 to 1
τ_{b^+}	Forward Transmittance at B interface, from 2 to 3
τ_{b^-}	Reverse Transmittance at B interface, from 3 to 2
ρ_{a^+}	Forward Reflectance at A interface, in media 1
ρ_{a^-}	Reverse Reflectance at A interface, in media 2
ρ_{b^+}	Forward Reflectance at B interface, in media 2

Figure 2.2 *Interfacial transmittance and reflectance coefficients*

location. The layer is of refractive index N_1 and physical thickness d interacts with a ray of light incident at an angle of θ_0. θ_0 is measured from the normal to the surface.

The reflected field is then

$$E_r = \rho_{a+}E_0 + \tau_{a-}\tau_{a+}\rho_{b+}e^{-i2\delta}E_0$$

$$+ \tau_{a-}\tau_{a+}\rho_{b+}^{2}\rho_{a-}E_0e^{-i4\delta} + \tau_{a-}\tau_{a+}\rho_{b+}^{3}\rho_{a-}^{2}E_0e^{-i6\delta}$$

$$+ \tau_{a-}\tau_{a+}\rho_{b+}^{4}\rho_{a-}^{3}E_0e^{-i8\delta} +\ldots+ \tau_{a-}\tau_{a+}\rho_{b+}^{p}\rho_{a-}^{p-1}E_0e^{-i2p\delta} . \qquad 2.38$$

In the infinite limit this reduces to

$$E_r = E_0\left\{\rho_{a+} + \frac{\tau_{a-}\tau_{a+}\rho_{b+}e^{-i2\delta}}{1-\rho_{a-}\rho_{b+}e^{-i2\delta}}\right\}. \qquad 2.39$$

Since

$$\tau_{a-}\tau_{a+} = 1-\rho_{a+}^{2} = \frac{4N_0N_1}{(N_0+N_1)^2} \qquad 2.40$$

and

$$\rho_{a-} = -\rho_{a+} \qquad 2.41$$

the reflection coefficient of a thin film is

$$\rho = \frac{E_r}{E_0} = \frac{\rho_{a+}+\rho_{b+}e^{-i2\delta}}{1+\rho_{a+}\rho_{b+}e^{-i2\delta}} . \qquad 2.42$$

Similarly the transmission coefficient is given by

$$\tau = \tau_{a+}\tau_{b+}e^{-i\delta} + \tau_{a+}\tau_{b+}\rho_{a-}\rho_{b+}e^{-i3\delta} + \ldots \qquad 2.43$$

$$= \frac{\tau_{a+}\tau_{b+}e^{-i\delta}}{1-\rho_{a-}\rho_{b+}e^{-i2\delta}} \qquad 2.44$$

$$= \frac{\tau_{a^+}\tau_{b^+}e^{-i\delta}}{1+\rho_{a^+}\rho_{b^+}e^{-i2\delta}} \quad . \qquad 2.45$$

The numerator contains the front and back surfaces acting independently whereas the denominator includes the effect of multiple reflections.

This treatment emphasizes the interfacial nature of a film. It is useful when analyzing the transient behavior of a film by considering a finite number of terms. An alternate approach, treats the steady state fields at the interfaces. Here the second interface, between the film and the substrate, is treated as a single interface, i.e., the substrate is assumed to be semi-infinite. At this location, denoted b in figure 2.2, the tangential components of E and H are,

$$\mathbf{H_b} = \mathbf{H_{1b^+}} + \mathbf{H_{1b^-}} = \eta_1(\mathbf{k}x\mathbf{E_{1b^+}}) - \eta_1(\mathbf{k}x\mathbf{E_{1b^-}}) \qquad 2.46$$

and

$$\mathbf{E_b} = \mathbf{E_{1b^+}} + \mathbf{E_{1b^-}} \quad . \qquad 2.47$$

Taking the cross product with respect to the propagation vector **k**, as we are interested in the fields perpendicular to the direction of propagation;

$$\mathbf{k} \times \mathbf{E_b} = \mathbf{k} \times \mathbf{E_{1b^+}} + \mathbf{k} \times \mathbf{E_{1b^-}} \qquad 2.48$$

and combining yields

$$2 \quad \mathbf{k} \times \mathbf{E_{1b^+}} = \frac{\mathbf{H}}{\eta_1} + \mathbf{k}x\mathbf{E_b}$$

$$2 \quad \mathbf{k} \times \mathbf{E_{1b^-}} = \frac{\mathbf{H}}{\eta_1} + \mathbf{k}x\mathbf{E_b} \quad . \qquad 2.49$$

The fields at the front interface, a, are determined by introducing a phase shift, $e^{\pm i\delta}$, due to traversal of the film. The negative exponent corresponds to the positive traveling wave while the positive applies to the returning wave. Thus :

$$E_{1a^+} = E_{1b^+} e^{-i\delta} \;;$$

$$K \times E_{1a^+} = \frac{1}{2}\left[\frac{H_b}{\eta_1} + K \times E_b\right] e^{-i\delta} \qquad 2.50$$

$$E_{1a^-} = E_{b_1^-} e^{i\delta}$$

$$K \times E_{1a^-} = \frac{1}{2}\left[-\frac{H_b}{\eta_1} + K \times E_b\right] e^{i\delta} \qquad 2.51$$

$$H_{1a^+} = H_{1b^+} e^{-i\delta} = \eta_1 K \times E_{1a^+} = \frac{\eta_1}{2}\left[\frac{H_b}{\eta_1} + K \times E_b\right] e^{-i\delta} \qquad 2.52$$

$$H_{1a^-} = H_{1b^-}\, e^{i\delta} = \eta_1 K \times E_{1a^-} = -\frac{\eta_1}{2}\left[\frac{H_b}{\eta_1} + K \times E_b\right] e^{i\delta} \;. \qquad 2.53$$

Now the above equations can be manipulated using Eulers relations to yield

$$k \times E_a = E_{1a^+} + k \times E_{1a^-} = k \times E_b \cos\delta + \frac{1}{\eta_1} H_b i \sin\delta$$

$$H = H_b + \eta_1 k \times E\, i \sin\delta \qquad 2.54$$

which can be expressed in matrix form as

$$\begin{bmatrix} k \times E \\ H \end{bmatrix} = \begin{bmatrix} \cos\delta & \frac{i}{\eta_1}\sin\delta \\ i\eta_1 \sin\delta & \cos\delta \end{bmatrix} \begin{bmatrix} k \times E_b \\ H \end{bmatrix} \;. \qquad 2.55$$

This matrix, due to Abeles (1950) , is known as the characteristic matrix and is used extensively in the calculation of thin film performance.

The above matrix equation can be simplified in form if we define the effective admittance of the assembly to be

$$Y = \frac{H_a}{kxE_a} . \qquad 2.56$$

The matrix equation above can then be recast as

$$kxE_a \begin{bmatrix} 1 \\ Y \end{bmatrix} = \begin{bmatrix} \cos \delta_1 & \frac{i \sin \delta_1}{\eta_1} \\ i\eta_1 \sin \delta_1 & \cos \delta_1 \end{bmatrix} \begin{bmatrix} 1 \\ \eta_2 \end{bmatrix} \quad kxE_b \qquad 2.57$$

This allows one to find the reflectivity of an interface between an incident medium with real admittance, η_0 and a thin film with admittance Y, by applying

$$\rho = \frac{\eta_0 - Y}{\eta_0 + Y} . \qquad 2.58$$

A case of particular interest is the quarter wave. This is a layer whose phase thickness, δ, at λ_0, is $\frac{\pi}{2}$. The optical properties of such a structure will have an extreme value whenever the thin film is of an odd number of quarter waves of optical thickness. At wavelengths for which it is an even number of quarter waves, referred to as halfwaves, the film will not affect the properties of the substrate. Halfwaves are thus referred to as absentee layers.

A layer of an odd multiple, m, of quaterwaves has a phase thickness $\delta = \frac{m\pi}{2}$, and the characteristic matrix reduces to

$$\begin{bmatrix} 0 & \frac{i}{\eta} \\ i\eta & 0 \end{bmatrix}. \qquad 2.59$$

For an even number of quarterwaves with no loss, $\delta = m\pi$ and the characteristic matrix becomes

$$\begin{bmatrix} \pm 1 & 0 \\ 0 & \pm 1 \end{bmatrix}. \qquad 2.60$$

MULTILAYER STACK

The extension of the previous calculations to the case of many layers is by induction. One starts in the exit medium and calculates the effect of each successive layer, treating the previous assembly as an effective substrate. This procedure is equivalent to forming the product of the characteristic matrices.

$$\begin{bmatrix} B \\ C \end{bmatrix} = \prod_{j=1}^{n} \begin{bmatrix} \cos\delta_j & \frac{i\sin\delta_j}{\eta_j} \\ i\eta_j \sin\delta_j & \cos\delta_j \end{bmatrix} \begin{bmatrix} 1 \\ \eta_s \end{bmatrix} \qquad 2.61$$

Where: $\delta_j = \frac{2\pi N_j}{\lambda} d_j \cos\theta_j$

$$\eta_j = \begin{matrix} N_j\cos\theta_j & \text{S polarization} \\ N_j/\cos\theta_j & \text{P polarization} \end{matrix} \qquad 2.62$$

and η_s is the substrate admittance.

The angle θ_j is determined from the incident angle θ_0 using Snell's law

$$\theta_j = \sin^{-1}\left[\frac{N_0}{N_j}\sin\theta_0\right]. \qquad 2.63$$

The admittance of the multilayer is defined as

$$Y=\frac{C}{B} \qquad \text{"free space units".} \qquad 2.64$$

Of prime concern in this work is the quarterwave stack, a structure consisting entirely of quarterwave layers. The admittance for a stack of n such layers on a substrate of admittance η_s, is readily found from equations 2.59 and 2.61 to be:

$$Y=\frac{\eta_1^2\ \eta_3^2\ \eta_5^2\ \ldots\ \eta_n^2}{\eta_2^2\ \eta_4^2\ \eta_6^2\ \ldots\ \eta_s}\ , \qquad 2.65$$

for n odd, and

$$Y=\frac{\eta_2^2\ \eta_4^2\ \eta_6^2\ \ldots\eta_n^2\ \eta_s}{\eta_1^2\ \eta_3^2\ \eta_5^2\ \ldots\ \eta_{n-1}^2}\ , \qquad 2.66$$

for an even number of layers.

In most standard designs two materials are used. The greatest reflectance for a given pair of materials is obtained when high index layers are used at the entrance and exit faces of the structure. This quarterwave stack contains p periods of alternating low index, η_l, and high index, η_h, plus a high index layer. The effective admittance of the multilayer is

$$Y = [\eta_h/\eta_l]^{2p}\eta_h^2/\eta_s\ . \qquad 2.67$$

For lossless dielectrics the possible reflectance is limited only by the number of layers deposited. Real layers have absorption and scatter. In low loss applications, such as mirrors for ring laser gyroscopes, the total loss can be less than 5 parts per million (Baumeister, 1986). The peak reflectance and shape of the mirrors response depends on the number of periods in the quarterwave stack, as shown in figure 2.3. These zones will exist wherever the layers are an odd

number of quarter waves thick (fig. 2.4). Born and Wolf find the full width at half of the maximum (FWHM) of this range to be independent of the number of layers,

$$\Delta\lambda = \frac{2}{\pi} \sin^{-1}\left[\frac{\eta_h-\eta_l}{\eta_h+\eta_l}\right] \lambda_0 , \qquad 2.68$$

depending only on the contrast of the high and low index materials.

Absorbing Multilayers

Thus far in our discussion we have considered only the ideal case of dielectric slabs. All real materials exhibit regions of strong absorption and one cannot always work far enough from these features to assure a negligible loss. A useful concept for the analysis of absorption (Berning & Turner, 1957) is that of potential transmittance. The potential transmittance of a layer , Φ, is defined as the ratio of the net radiation flux emerging to the amount actually entering the layer,

$$\Phi \equiv \frac{T}{1-R} = \frac{T}{T+A} = \frac{1}{1+\frac{A}{T}} \qquad 2.68$$

It depends only on the properties of the exiting media and the layer.

For weakly absorbing layers (k/n<<1), with reasonable phase thickness (δ'), the change in potential transmittance can be approximated by

$$\Phi-\Delta\Phi = 1- 2\Gamma[\, f\delta'+ g\sin(\delta'\cos(\xi+\delta'))] , \qquad 2.69$$

where $f = \dfrac{1+|\rho_b^-|^2}{1-|\rho_b^-|^2}$,

(A)

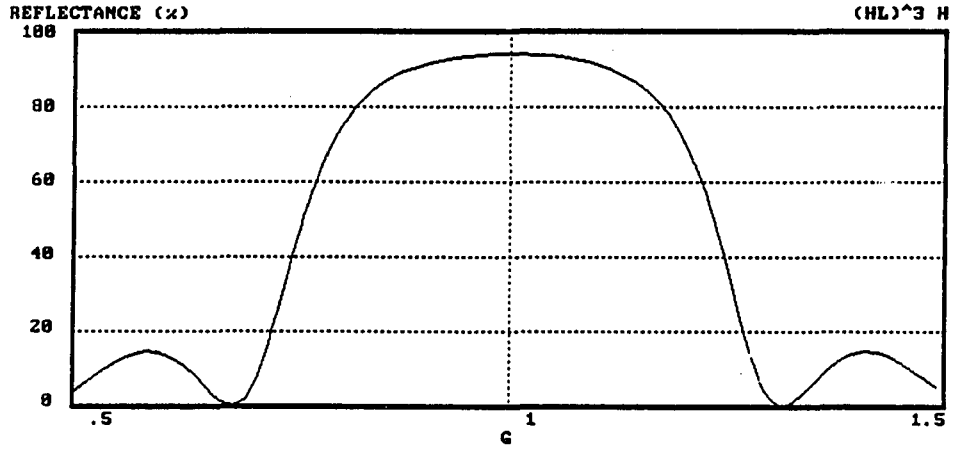

(B)

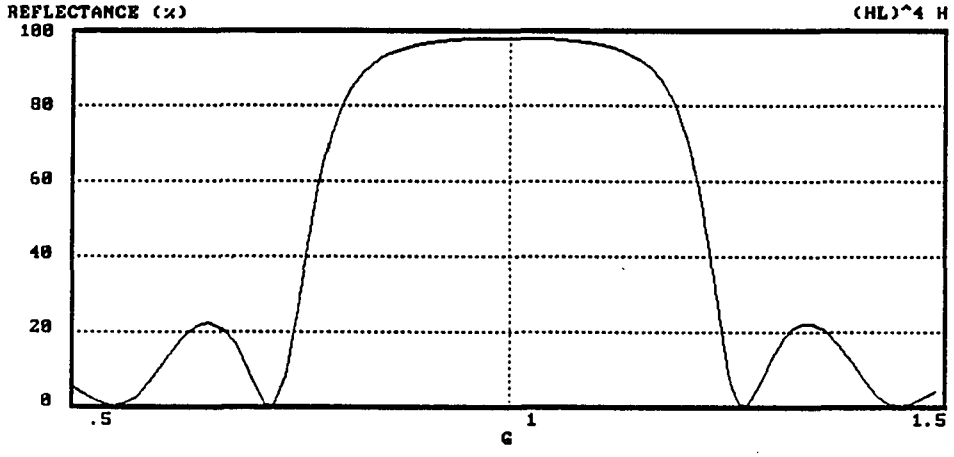

(C)

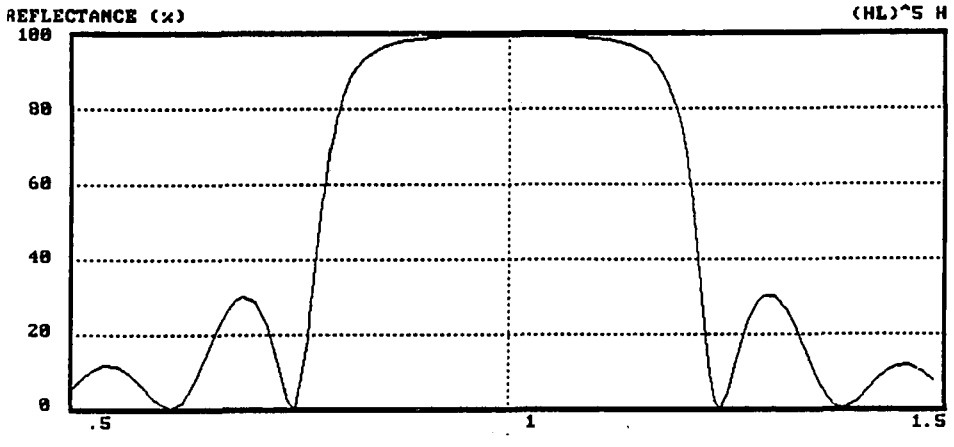

Figure 2.3 *The reflectivity of a multilayer stack* ;

for three different periods, p, of the high reflectance configuration glass| $(hl)^p h$ | glass, (A) p=3, (B) p=4, (C)p=5.

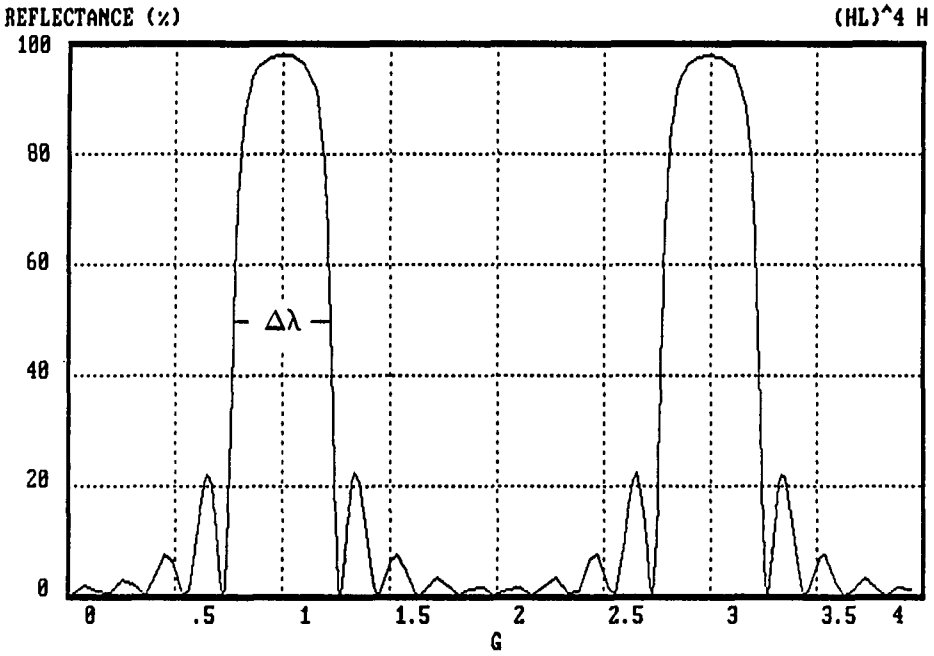

Figure 2.4 *The zones of high reflectance*

Calculated in terms of $G=\frac{\lambda_0}{\lambda}$ and λ_0 is the design wavelength.
In this illustration the period,p of the stack is 4.

and $$g = \frac{2|\rho_b^-|^2}{1-|\rho_b^-|^2} .$$

Hemmingway & Lissberger (1973) extended this work and state that this equation is valid for the conditions

$$\Delta\Phi < .1 \quad \text{or} \quad |\rho|^2 < 1-40\Gamma\delta'. \tag{2.70}$$

If this relation is valid for each layer independently, then the potential transmittance of a multilayer structure is found by expanding the product of potential transmittance and retaining only the linear terms. Thus

$$\Phi_m = 1-\Delta\Phi_m \tag{2.71}$$

with,

$$\Delta\Phi_m = \sum_{i=1}^{m} \Delta\Phi_i \tag{2.72}$$

and

$$\Delta\Phi_i = 1-\Phi_i . \tag{2.73}$$

Let the transmittance, absorptance and reflectance of a multilayer of m layers be denoted T_M ,A_M and R_M respectively. The potential transmittance is then

$$\Phi_M = \frac{T_M}{1-R_M} = 1-\frac{A_M}{1-R_M} . \tag{2.74}$$

When such a stack consists of 2p+1 alternating layers of high and low index material then the absorptance is found to be, in terms of the refractive indices :

$$A_m = \frac{2\pi(n_l/n_h)}{1-(n_l/n_h)^2}\left[\left[\frac{1-(n_l/n_h)^{2p+2}}{1+(n_l/n_h)^{2p+2}}\right]\left[\frac{k_h}{n_h}\right]+\left[\frac{1-(n_l/n_h)^{2p}}{1+(n_l/n_h)^{2p+2}}\right]\left[\frac{k_l}{n_h}\right]\right] . \tag{2.75}$$

In most cases of interest this can be approximated as

$$A_m = \frac{2\pi\, n_l}{n_h - n_l} \left[\frac{k_h + k_l}{n_h + n_l} \right] . \qquad 2.76$$

This is the basic result for a lossy mirror of 2p+1 layers. It shows that the absorptance of a multilayer reflector is independent of the number of layers, provided there are enough of them (approximately 7 layers for ZnS and chiolite). The reflectance of a multilayer tends to $1-A_m$ instead of 1 as the number of layers is increased. This effect can be readily understood if one considers the rapid decrease of the field amplitude in a mirror (figure 2.5).

Narrow Band Filters

Narrow band optical filters (NBF), whether of metal dielectric or all dielectric design, are Fabry-Perot etalons with a fixed spacer thickness determined by the product of physical thickness and refractive index. Dielectric NBF's are ideally lossless. However, a lossless filter presents no mechanism for thermally induced bistability.

The Fabry-Perot interferometer (1899) consists in its most basic configuration of two flat plates separated by an air spacer. The characteristic performance of such a device is found in much the same manner as a single layer of material above. The transmission is found to be

$$T = \frac{I_t}{I_i} = \frac{|\tau_{a^+}|^2 |\tau_b^-|^2}{(1-|\rho_{a^-}||\rho_{b^+}|)^2} \frac{1}{1+\frac{4|\rho_{a^-}||\rho_{b^+}|}{(1-|\rho_{a^-}||\rho_{b^+}|)^2} \sin^2\left[\frac{\xi_a + \xi_b + 2\delta}{2}\right]} . \qquad 2.77$$

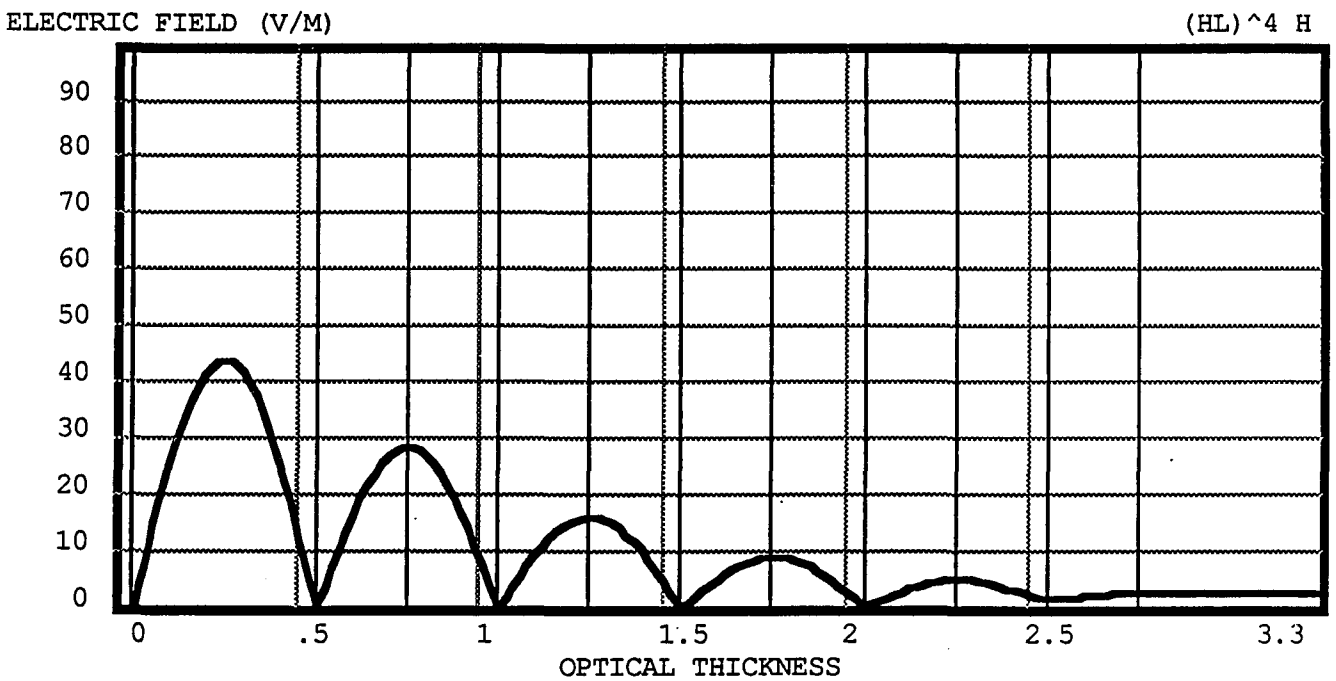

Figure 2.5 *Electric field in a mirror* , an all dielectric mutilayer design as figure 2.4, normalized to 1 $\frac{\text{watt}}{M^2}$ incident for G=1.

If the phase change on reflection is assumed to be identical for both reflectors, and is small compared to the phase thickness of the etalon, one can set $\xi_a = \xi_b = 0$. The spacer is air in a traditional Fabry-Perot etalon, $\eta_s = 1$, and

$$T = \frac{T^2}{(1-R)^2} \frac{1}{1+\frac{4R}{(1-R)^2}\sin^2\delta} . \qquad 2.78$$

Figure 2.6 shows the transmittance function of a Fabry-Perot etalon as a function of the endmirror reflectivity

Let

$$\mathcal{F} = \frac{4R}{(1-R)^2} , \qquad 2.79$$

be the coefficient of finesse, then

$$T = \frac{T^2}{(1-R)^2} \frac{1}{1+\mathcal{F}\sin^2\delta} \qquad 2.80$$

the first term, $\frac{T^2}{(1-R)^2}$ is an amplitude term, the second term is the "Airy function". If we have ideal dielectrics then T=1-R, and

$$T = \frac{1}{1+\mathcal{F}\sin^2\delta} . \qquad 2.81$$

This quantity has a maximum whenever $\delta = m\pi$, and a minimum whenever $\delta = \left[m+\frac{1}{2}\right]\pi$, where m is an integer. In the ideal case the transmittance of an etalon is independent of the reflectivities of the mirrors. The width of this function is inversely proportional to F. As the reflectance increases the fringes become narrower.

The most common quantity in defining the performance of such a device is the full width at half maximum (FWHM), $\delta_{1/2}$. It is defined as the value of

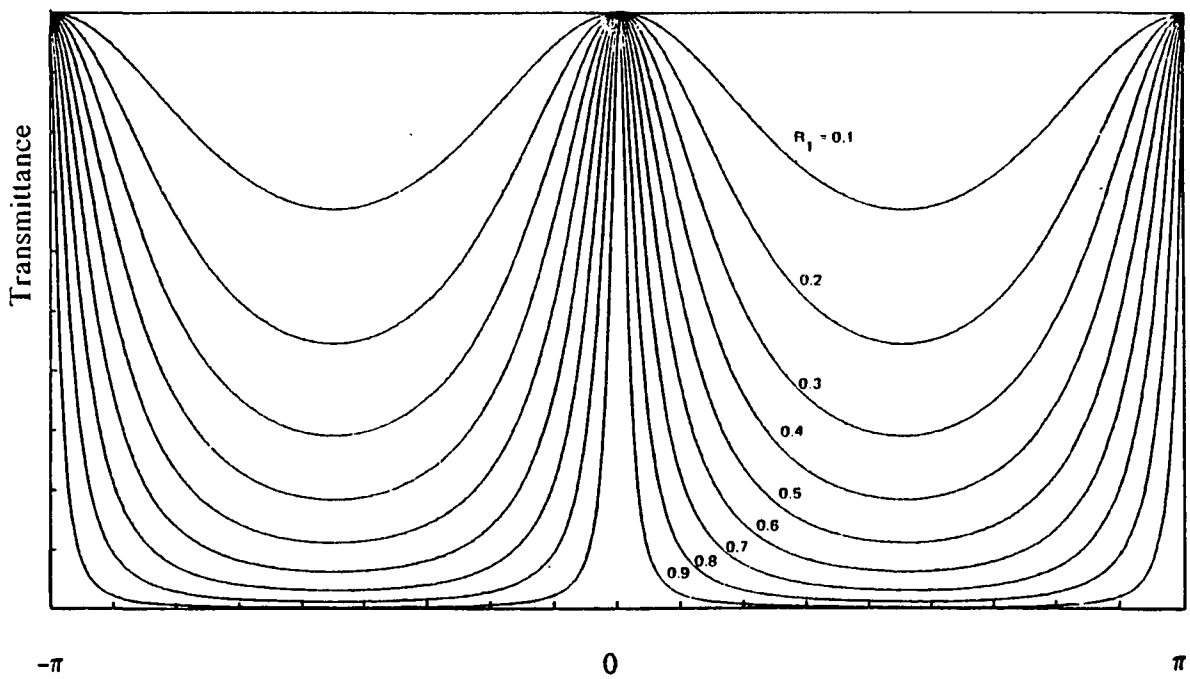

Figure 2.6 *The Transmittance function of a Fabry-Perot Narrow Band Filter* as a function of phase for various reflectivities. The cavity is assumed losseless.

phase, δ, for which the transmission has decreased to one half its peak value. Thus

$$\delta_{1/2} = \sin^{-1}\left[\frac{1}{\sqrt{F}}\right] \cong \frac{1}{\sqrt{F}}\ , \qquad 2.82$$

is often expressed as a percentage by dividing by the peak wavelength, $\frac{\delta_{1/2}}{\lambda_0}$.

In etalons the phase change from reflection is small in comparison to the spacer phase thickness and can thus be neglected. In NBFs the phase change on reflection cannot be ignored, as the phase dispersion in the mirrors is of the same order of magnitude as the phase change in traversing the spacer.

Seeley (1964) has shown that a significant narrowing of the halfwidth results from this phase dispersion. As the dielectric reflectors are assumed to be of the highest reflectance configuration, there are two cases of interest. The structure is assumed to be surrounded by a non-absorbing media, n_i. These two cases are:

A high index spacer,

$$\Delta\lambda_{1/2} = 4\ n_i n_l^{2p} \frac{n_h - n_l}{m\pi n_h^{2p+1}\ (n_h - n_l + n_{l/m})}\ ; \qquad 2.83$$

and a low index spacer,

$$\Delta\lambda_{1/2} = 4 n_i n_l^{2p-1}\ \frac{n_h - n_l}{m\pi n_h^{2p}\ (n_h - n_l + n_l/m)}. \qquad 2.84$$

where: m is the order number of the spacer

p is the number of periods in the stack

with high n_h,and low n_l, index material

Absorption Losses in Narrow Band Filters

A Fabry-Perot narrow band filter of the lowest order can be considered as two reflecting stacks (as above) connected by an infinitely thin layer of refractive index n_h. For symmetric stacks of equivalent potential transmittance Φ_m, the transmittance is obtained from the Airy formula as

$$T = \frac{\Phi_m^2}{1 + F\sin^2\phi} . \qquad 2.85$$

Over the passband of the filter the potential transmittances of the individual layers change slowly and the maximum transmittance of the filter can be expressed as

$$T_{max} = \Phi^2_m = 1-2\Delta\Phi_m . \qquad 2.86$$

The quantity $2\Delta\Phi_m$ represents the decrease in peak transmission of a narrow band filter due to attenuation:

$$2\Delta\Phi_m = \pi\left[\frac{k_h}{n_h}\right]\frac{1+r}{1-r}\left[\mu + \frac{(n_l/n_h)^2}{1-(n_l/n_h)^2} + \frac{(n_l/n_h)^2}{1-(n_l/n_h)^2}\,\frac{k_l n_h}{k_h n_l}\right] . \qquad 2.87$$

In terms of the fractional halfwidth, $\Delta\lambda/\lambda$, absorption of the filter is

$$2\Delta\Phi_m = 4\left[\frac{k_h}{n_h}\right]\frac{\left[\mu + \frac{(n_l/n_h)^2}{1-(n_l/n_h)^2} + \frac{(n_l/n_h)^2}{1-(n_l/n_h)^2}\,\frac{\frac{k_l}{n_l}}{\frac{k_h}{n_h}}\right]}{\frac{\Delta\lambda}{\lambda}\left[\mu + \frac{n_l/n_h}{1-(n_l/n_h)}\right]} \qquad 2.88$$

where $\frac{\mu\lambda_0}{2}$ is the optical thickness of the spacer.

For a specified filter halfwidth the change in potential transmittance due to spacer thickness is positive if

$$k_h n_l > (k_l n_h) \ . \qquad 2.89$$

Filters for which this applies should be of the lowest order if high transmittance is required.

Oblique Incidence

In order to obtain sufficient flux and the proper peak location of the filter to observe optical bistability it is necessary to use the filters in a focused beam at slightly oblique incidence. Lissberger (1959), and Pidgeon and Smith (1964), have analyzed the performance of first order filters for collimated non-normal and convergent illumination. In oblique collimated illumination the peak transmittance shifts to shorter wavelengths. The authors show that the shift can be accurately predicted, for angles less than 20^0, by considering the filter as a single layer of effective admittance determined :

$$n_h^* = \sqrt{n_h n_l} \qquad \text{for a high index spacer} \qquad 2.90$$

and

$$n_l^* = \sqrt{\frac{n_l^2}{1-(n_l/n_h) + (n_l/n_h)^2}} \quad \text{for a low} \ . \qquad 2.91$$

Let

$$\lambda_{peak} = \lambda_0 \cos\theta = \lambda_0 - \Delta\lambda \qquad 2.92$$

where

$$\theta = \sin^{-1}(n_i \sin\theta_i / n^*) \qquad 2.93$$

then for small angles

$$\Delta\lambda \cong \frac{\theta_i^2}{2n^{*2}}\lambda_0, \qquad 2.94$$

and the angle θ is in radians.

Figure 2.7 shows the effect of tilting a filter.

Macleod(1986) has extended this work for higher order (m) spacers finding:

$$n^* = n_h \sqrt{\frac{[m-(m-1)(n_h/n_l)]}{[(m-1)-(m-1)(n_l/n_h)+(n_h/n_l)]}} \qquad 2.95$$

for high index spacers;

$$n^* = n_l \sqrt{\frac{[m-(m-1)(n_l/n_h)]}{[m-m(n_l/n_h)+(n_l/n_h)^2]}} \qquad 2.96$$

which reduce to the above for first order cavities.

Pidgeon and Smith show, in terms of wavenumbers (cm^{-1}), $1/\lambda$, that if such a filter is used in converging illumination, of semiangle ζ, then the transmittance band is determined by averaging the transmittance function over all angles from normal incidence to ζ. Such an averaging must cause a reduction in the performance of the filter since it is essence a convolution. One naturally expects that the peak transmittance will be reduced as well as shifted and the halfwidth increased.

The total transmitted flux is proportional to

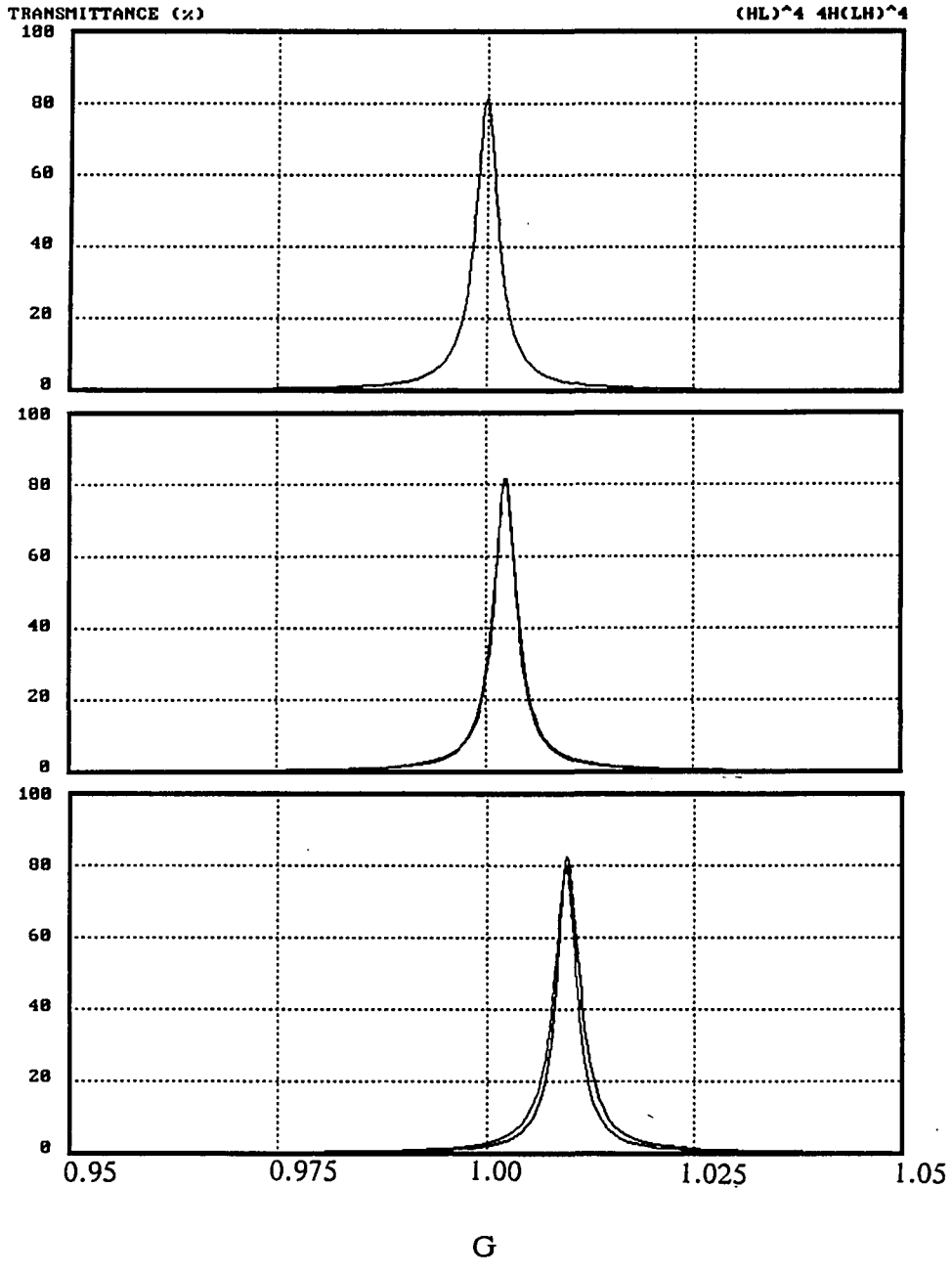

Figure 2.7 *The change in transmittance for small change in angle.*

(a) normal incidence, (b) θ=5^0,(c) θ=10^0.

$$\int_0^{\zeta} \zeta T d\zeta \ . \qquad 2.97$$

This function is maximized when

$$\Delta g = \frac{1}{2} \frac{\zeta^2}{2n^{*2}}. \qquad 2.98$$

The new peak wavelength is shifted to the average of the normal incidence value and at an angle ζ.

The value of the new peak transmittance is

$$T = \frac{2\Delta g_{1/2} n^{*2}}{\zeta^2} \tan^{-1}\left[\frac{\zeta^2}{2n^{*2}\Delta g_{1/2}}\right]. \qquad 2.99$$

and the halfwidth (fwhm) is found to be

$$\Delta g'_{1/2} = \sqrt{\Delta g_{1/2}^2 + \left[\frac{\zeta^2}{2n^{*2}}\right]^2}. \qquad 2.100$$

The fractional halfwidth of an interference filter increases with the convergence angle.

The linear characteristics of Fabry Perot filters, either ideal or lossey are predicted accurately through classical electromagnetic theory. This requires only that the "optical constants" of the material be accurately known. For real thin films these constants vary with process parameters and their determination from the observed reflectance or transmittance is non-trivial.

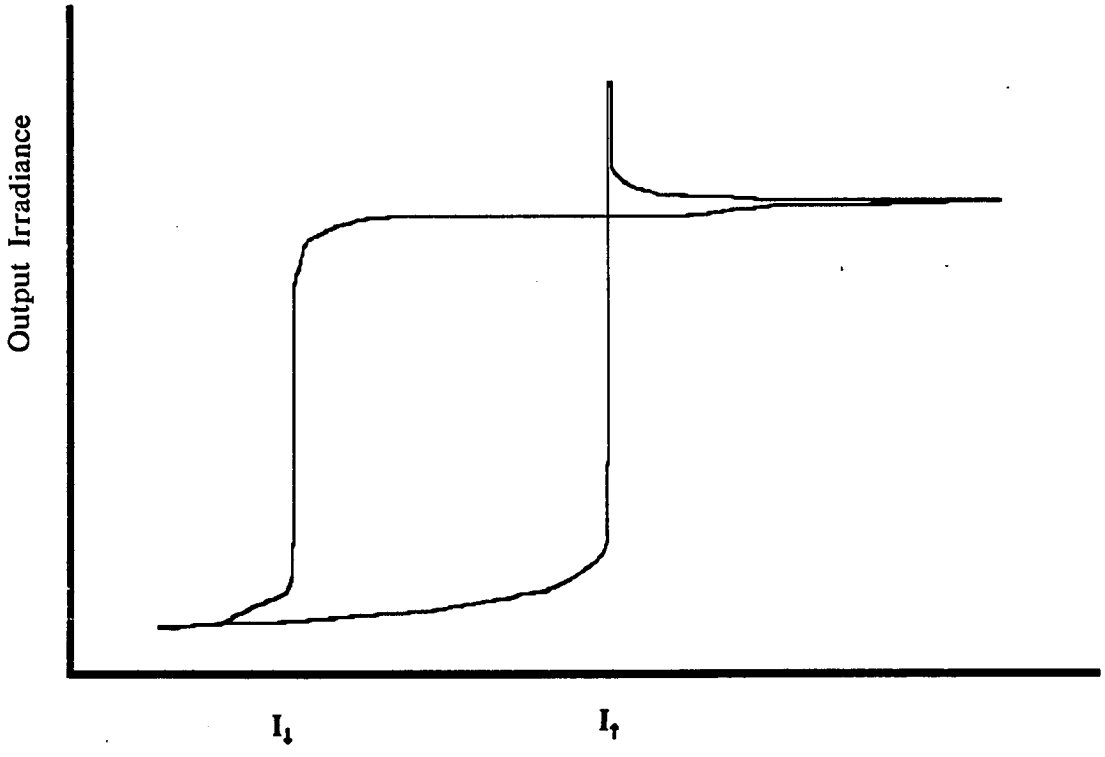

Figure 3.1 *Idealized hysteresis loop for a bistable device.*
I_{out} the output irradiance as a function of input irradiance I_{in}. $I_\uparrow$ is the switch up irradiance, $I_\downarrow$ the switch down irradiance, they bound the bistable region.

OPTICAL BISTABILITY

This chapter reviews the field of optical bistability with emphasis on the material relevant to our NBFs. For a more general and detailed description of bistability the reader is directed to Gibbs (1986).

An optical system is said to be bistable if over some range of inputs a single value of the input has two stable outputs. The two states in an optically bistable system are defined either by the transmitted or reflected irradiance, I_{out}, as a function of the input irradiance, I_{in}. As the output irradiance depends on the proceeding state of the device, a hyterises loop is obtained. (figure 3.1) In this figure the bistable region is between the switch down irradiance, $I_{\downarrow}$ and the switch-up irradiance $I_{\uparrow}$.

There are two fundamental requirements for bistability. These are the presence of nonlinearity and feedback. A system that has gain is said to be active, otherwise it is passive. All-optical (intrinsic), as well as hybrid (containing electro-optic), elements have been investigated. For our work the case of passive intrinsic bistability is of interest. All further references to optical bistability are to all-optical systems that do not exhibit gain.

Optical bistability (OB) is categorized by the underlying physical process from which the nonlinearity results. Four such categories are dispersive (Mccall et al 1976), absorptive (Szöcke, 1969; Seidel, 1969), increasing absorptive (Toyozawa, 1978), and mechanical (Dorsel et al 1981).

The case of absorptive bistability offers a convenient starting point for this discussion. Szöcke and Seidel independently predicted that a saturable absorber placed in a resonant cavity would produce hysteresis. A saturable absorber is a material which has an intensity dependent absorption coefficient (Sargeant, Scully and Lamb). When illuminated at resonance this type of material becomes transparent, i.e. at some intensity I_s the absorption saturates. The intensity dependent absorption coefficient is of the form

$$\alpha = \frac{\alpha_0}{1+\frac{I}{I_s}}. \qquad 3.1$$

When a saturable absorber is placed in a Fabry-Perot cavity it eliminates the feedback for low input power. This lack of feedback isolates the first mirror and destroys the cavity finesse. As the input power is increased the absorption decreases and a greater proportion of the incident field traverses the cavity and returns to the first mirror. The returning field incident at the first mirror destructively interferes with the incident beam. This interference increases the flux transmitted into the cavity, and positive feedback is established. The energy density in the cavity thus increases, eventually saturating the medium. For input larger then the saturation intensity the cavity behaves linearly. It transmits all the incident power that is not lost to non-resonant absorption or scatter.

When the input power is subsequently decreased the fields in the cavity remain large due to the low transmittance of the mirrors. The media remains bleached after the input power falls below the switch-up point ($I_\uparrow$) and all of the incident power is transmitted. As the input power is decreased further the energy density in the cavity falls below I_s, the threshold at which resonant absorption is

significant. This absorption depletes the reflected amplitude, reducing the interference and the transmission collapses rapidly to a low level.

This sort of saturable absorption bistability has been difficult to observe, due in part to non-saturable non-resonant absorption which is usually present. Such background absorption increases the power required and decreases the contrast between the high and low transmission states.

The process of increasing absorptive bistability is essentially the inverse process of the proceeding absorptive case. Here the material is initially only slightly absorbing, and illumination creates free carriers, electrons and holes, which increase the absorption coefficient of the material. This increases the amount of light absorbed, producing more carriers. The hysteresis is provided through the finite carrier lifetime. There is, in this case, no need for external feedback. Instead, one must have absorption with a greater than linear dependence on the carrier density.

Mechanical bistability (Dorsel et al, 1981) is a radiation pressure driven form of bistability. An etalon consisting of a fixed mirror and a light mirror (60 mg) mounted as a pendulum, is irradiated off resonance. The radiation pressure pushes the pendulum bringing the device into resonance by changing the separation of the plates. Hence the device switches on. The beauty of this experiment is the macroscopic manifestation of a quantum mechanical effect.

Until 1976, when Gibbs, McCail and Venkatesan observed bistability in Na vapor which was inconsistent with an absorptive model, all descriptions of intrinsic optical bistability were of the absorptive type. In their work, a combined absorptive and dispersive model of bistability is described. Dispersive bistability results from an intensity dependent change in refractive index. It is a

temperature dependent dispersive effect which produces the bistability in the Fabry-Perot NBFs we have been investigating.

Dispersive bistability is described in terms of an equilibrium model. The boundary conditions are illustrated in figure 3.2. The incident field (E_i), forward travelling wave (E_f), and transmitted (E_t) fields are related via:

$$E_t = \tau E_f(l) \ , \qquad 3.2$$

and they are;

$$E_f(0) = \tau E_i + R e^{-\alpha l + i\beta} E_f(0) \ . \qquad 3.3$$

Here: τ is the amplitude transmitance ; and, $R = |\rho|^2$, the intensity reflectance of the identical endmirrors is used because this is the field after a complete round trip in the cavity, i.e. after the field has been reflected off the interior face of the first mirror. The mirrors are assumed linear, lossless, and any phase change on reflection is incorporated into β. The cavity is characterized by the parameters: $\alpha = 4\pi k/\lambda$, the intensity absorption coefficient; β the cavity-laser detuning; and l, it's physical length. These boundary conditions apply to the general case of combined absorptive-dispersive bistability. For purely absorptive bistability, the frequency of the laser and cavity are matched, i.e. $e^{i\beta} = 1$. In purely dispersive bistability, one ignores the absorption term by setting α equal to zero while retaining the phase term $e^{i\beta}$. Then equation 3.2 becomes

$$\frac{E_{f(0)}}{E_i} = \frac{\tau}{1 - |\rho| e^{i\beta}} \ . \qquad 3.4$$

The transmitted wave is

$$E_t = \frac{\tau e^{i\beta}}{2} E_f(0), \qquad 3.5$$

and the incident wave is

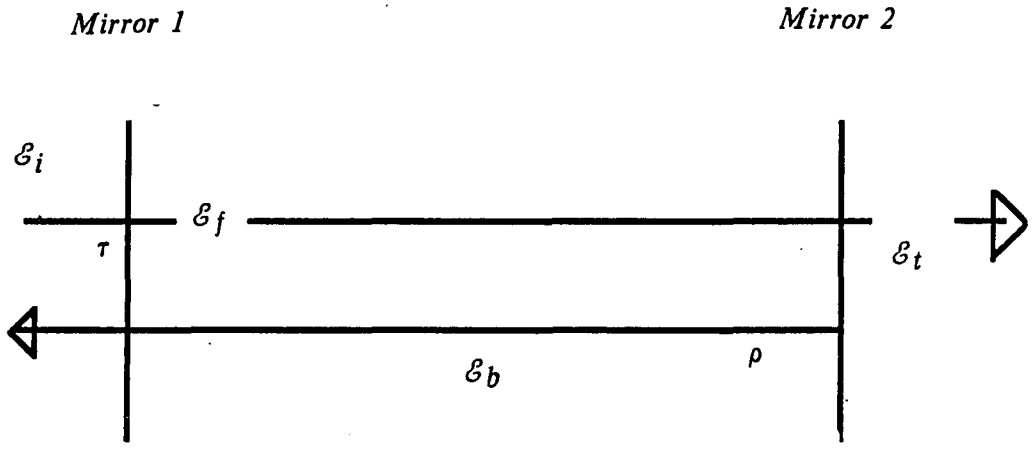

$\mathcal{E}_i$, incident field;
$\mathcal{E}_f$, forward traveling electric field inside the cavity;
$\mathcal{E}_b$, returning wave inside the cavity;
$\mathcal{E}_t$, the transmitted field.

Mirrors one and two are assumed to be identical with reflectivities ρ and transmittance τ.

Figure 3.2 *A schematic representation of a Fabry-Perot etalon*

$$E_i = \frac{(1-Re^{i\beta})E_t}{\tau^2 e^{i\beta/2}} . \qquad 3.6$$

Incident and transmitted intensities are found to be functionally related by

$$I_i = I_t \frac{|1-Re^{i\beta}|^2}{\tau^4} . \qquad 3.7$$

The exponential is expanded, assuming R>>T, and only the terms quadratic in β are retained, to yield :

$$I_i = I_t(1+\beta^2/T^2). \qquad 3.8$$

Here,

$$T=\frac{I_t}{I_i} \qquad 3.9$$

is the intensity transmittance.

Let the phase shift be intensity dependent, and of the form

$$\beta=\beta_0+\beta_2 I_t, \qquad 3.10$$

where β_0 contains all the intensity independent contributions.

For bistability one requires that $\frac{dI_t}{dI_i} < 0$, i.e that the device is driven past the peak transmittance. Solving for the inflection point one finds that

$$|\beta_0| > \sqrt{3}\frac{T}{R} = \sqrt{3}\frac{\pi}{\mathcal{F}} . \qquad 3.11$$

$\mathcal{F} = \frac{4R}{1-R^2}$ is the cavity coefficient of finesse.

Together equations 3.9 and 3.10 provide a parametric solution for the behavior of a nonlinear NBF which is found graphically (Malberger and Felber, 1978). Where, I_t, I_i are the transmitted and incident irradiances and T_0 is the

peak transmittance of the filter. Figure 3.3 shows two solutions that form the bounds for bistability in a resonant device. The curved line represents the transmission of the device as a function of the phase difference. The two straight lines, A and B, are solutions to

$$\frac{I_t}{I_i} = \frac{\beta-\beta_0}{\beta_2 I_i} \qquad 3.12$$

for two input irradiances bounding the region in which bistability is observed. Load line A is the "critical irradiance" defined as the minimum power that intersects the response curve at three points, two of which are stable. "A" intersects the axis at β_c and is the critical minimum detuning. The slope of load line B is determined by the maximum power that is applied to the device. The shape of the filter's transmittance and the slope of B determine β_m, the maximum initial detuning. The region bounded on the axis by β_c and β_m encompasses the useful range of the device.

Figure 3.4 illustrates the operating characteristics of a bistable etalon. The switch-up and switch-down irradiances are determined from the intersection of the load lines with the filter's transmittance function. If B is the highest irradiance (minimum slope) load line, then β_b is the maximum initial detuning for which bistability is possible. The slope of A is inversely proportional to the switch down irradiance. The difference between the two slopes determines the range of irradiances for which the device has two stable outputs. The instability of point b_2 is seen by considering the effect of a small change in the input irradiance. The slope of the response curve, and thus the feedback, is positive. Therefore, the device will be driven away from this solution to the region where the feedback is negative.

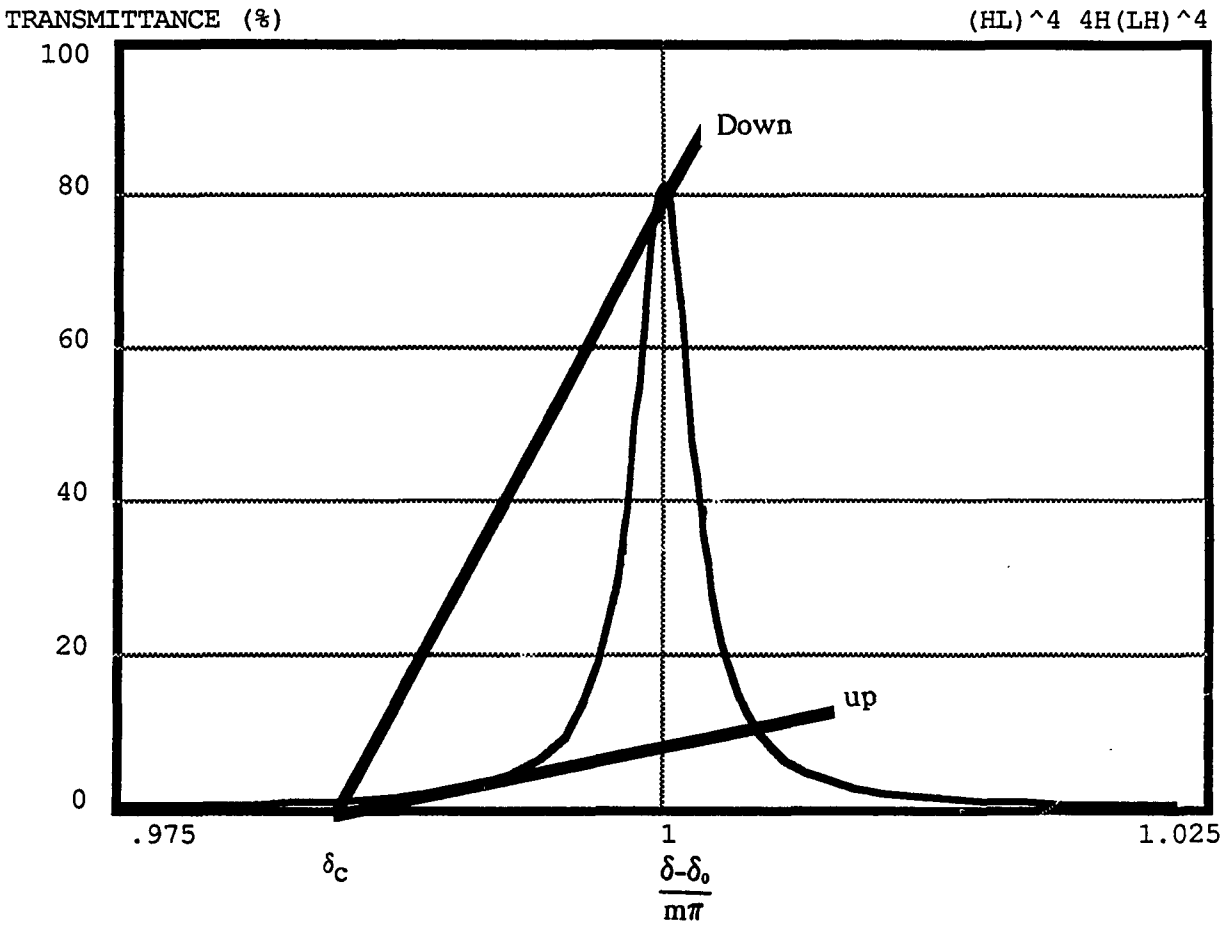

The Switch up (up) and switchdown (down) load lines, (I_t/I_i) for a standard Fabry Perot filter design. The point where the two lines meet at the phase axis is δ_c the initial detuning.

Figure 3.3 *Graphical solution of switching characteristics*

Nonlinear Fabry Perot Filters and Bistability

Non-linear effects are observable in thin film etalons because of electric field enhancement of the cavity. This resonant enhancement arises from the confinement of the field between two highly reflecting mirrors. The light is thought of as bouncing back and forth in the cavity many times before it leaks out. In figures 3.5 a,b,c the electric field in a slightly absorbing NBF is shown as a function of the propagation direction z. The three cases depict the change from off to on resonance. The filter design in this figure is $(HL)^4 4H(LH)^4$ with refractive indices are $H=2.35-i5\times10^{-4}$ and $L=1.35$.

Theory of Bistability in Thin Film Etalons

Bistability in ZnS thin film etalons is produced by an indirect intensity dependent change in the spacer thickness. Zinc sulfide has a refractive index which increases with temperature. Background absorption in a NBF causes heating which is proportional to the incident flux. This results in a refractive index that is written as

$$N=n_0+n_2I. \qquad 3.13$$

Bistability in ZnS is essentially dispersive as the absorption does not saturate. The switch from low to high transmission is a result of the incident light increasing the optical thickness of the cavity. This process is a balance between heat pumped into the filter and heat lost to the surrounding media.

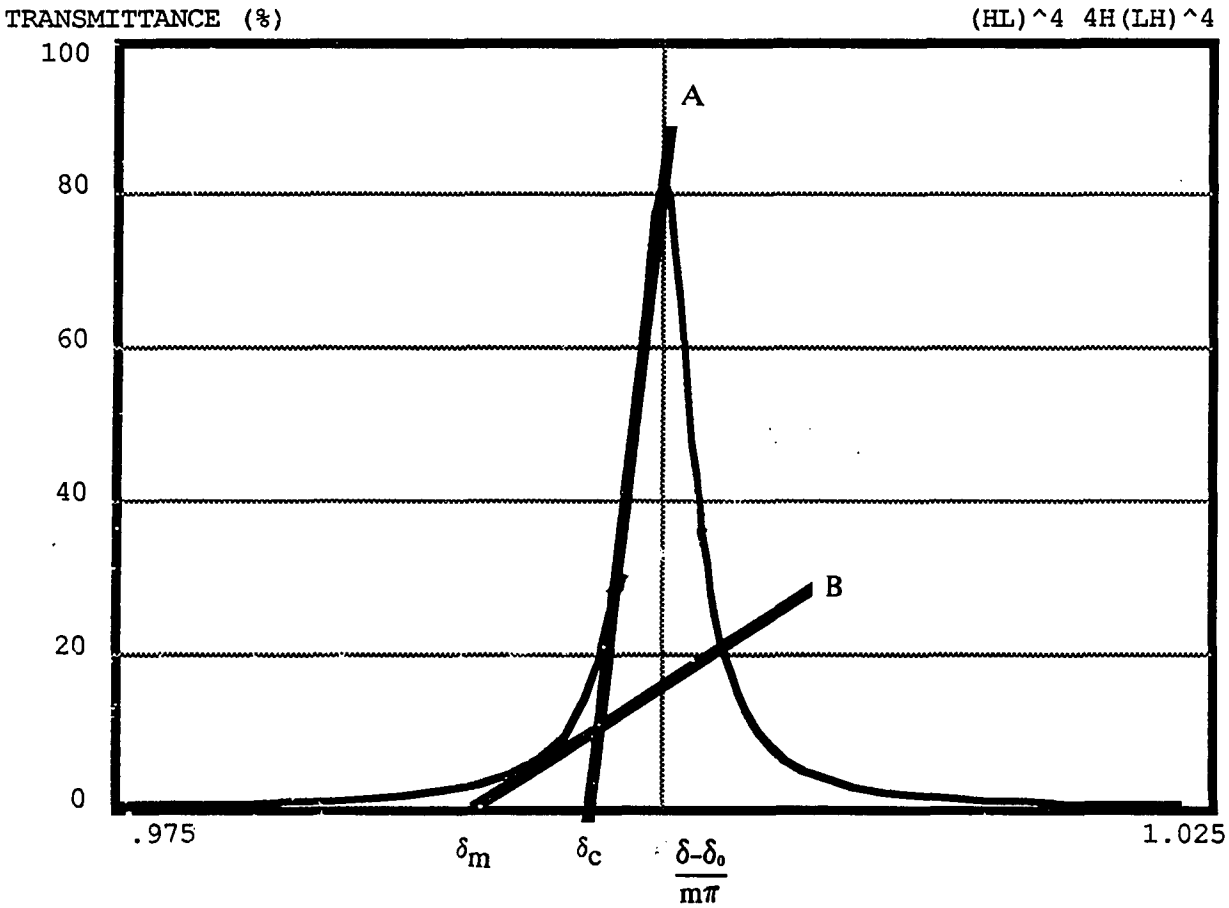

Figure 3.4 *The Region over which bistability is observable*

The graphical solution for bistability shows the region over which thermal refractive bistability is observable. Load line A is the critical irradiance below which the function is single valued. B is the irradiance level at which damage to the filter occurs.

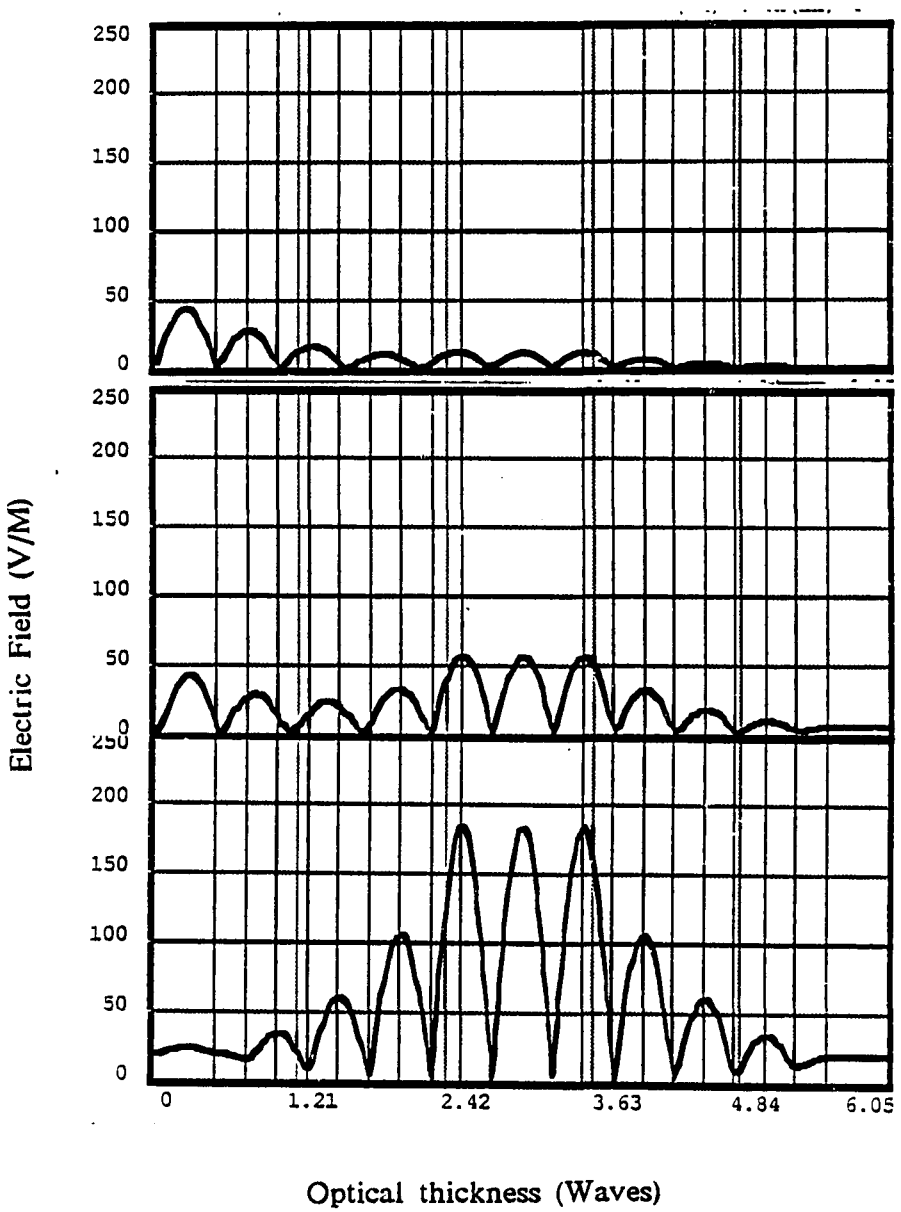

Figure 3.5 *The electric field in a single cavity filter*

normalized to 1 W/M² incident power density, as the filter switches from off to on resonance.

The first observers of nonlinearity in thin film etalons (Karpusko et al, 1977, 1978, 1983) attributed the nonlinearity to two photon photorefraction. Olbright et al (1984) have since shown that a thermal mechanism is responsible for the bistability. The thermal mechanism is indicated by the lack of strong excitonic peaks in the spectrum of ZnS at room temperature and the relative wavelength dependence of the NBF's performance.

The spacer thickness in a Fabry-Perot NBF determines the peak wavelength of the device and has a weak influence on the FWHM. The reflectivity of the dielectric mirrors strongly affects the peak transmittance and width. Since the wavelength of the filter is directly determined by the optical thickness of the spacer layer, a small change in it's properties is easily detected through the shift in wavelength. The reflectivities of the mirrors are a comparatively slowly varying function, as is seen from figure 3.6. It is therefore reasonable to assume that the reflecting stacks are effectively unchanged during switching and that the performance of the multilayer is reduced to consideration of the spacer layer alone.

The change in optical path length (Δopl) due to a finite change in the temperature is written as :

$$\frac{\Delta opl}{\Delta T} = \frac{\Delta(NL)}{\Delta T} = \frac{L\Delta N}{\Delta T} + \frac{N\Delta L}{\Delta T}. \qquad 3.14$$

For a spacer of one wave optical thickness at 633 nm Olbright (1984) reports

$$L\Delta N/\Delta T \text{ of } .075 \text{ nm}/^{0}C$$

and

$$N\Delta L/\Delta T \text{ of } .004 \text{ nm}/^{0}C. \qquad 3.15$$

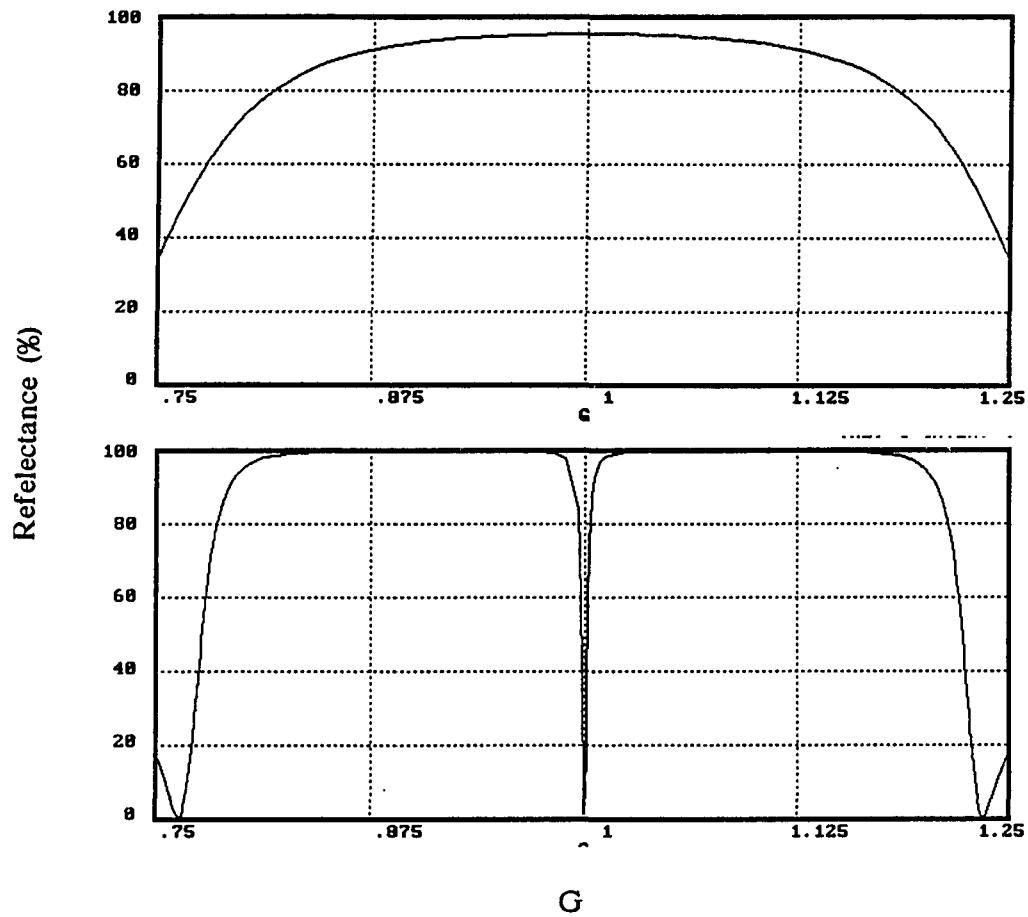

Figure 3.6 *The Reflectance of a NBF compared to that of its mirrors*

One sees that the refractive index change with temperature dominates the thermal expansion. The thermal expansion is therefore neglected.

If the energy stored in a volume V of the cavity is

$$E=\rho C_p \, V\Delta T \qquad 3.16$$

where: ρ is the mass density

C_p is the heat capacity

V is the volume

ΔT the change in temperature required to switch the device.

Then, ignoring heat flow, the switch on time, τ, is $\frac{E}{\alpha P}$. Here α is the absorption coefficient and P the mean cavity power. Combining with 3.16, one finds

$$\tau=\frac{\rho C_p}{\alpha P} \, V\Delta T. \qquad 3.17$$

The minimum time for switching is inversely proportional to the power and significantly, monotonic with volume. Therefore, if the element to be switched is made small this characteristic time will also be small. This indicates one way in which the performance of a switching element is improved. Another observation from this equation is that, since both ρ and α are directly related to the structure of a thin film, as the porosity increases the density decreases and the absorption increases. The porosity also reduces the heat flow through the film. Thus a "poor" film should have a faster characteristic time, at the expense of high transmittance.

More generally the optimization of switching characteristics for a thermally refractive bistable element has been studied. Brian Wherret (1984), Wherret, Hutchings, Russel (1986), and D.A.B. Miller (1981) studied the effects of

spot size, radiation frequency, and design parameters on a standard Fabry-Perot filter used in transmission or reflection. A standard design consists of quarterwave stack mirrors and an m halfwave spacer. It should be noted before this discussion that thin films do not exactly mimic bulk behavior. Thermal conductivity is lower, the band edge broader, and both are likely to depend on thickness. Film interfaces have residual absorption, scatter, and may impose thermal impedance, so that interfilm conductivity is lower than intrafilm. These parameters are highly dependent on the manufacturing conditions of a particular thin film. These complications make direct quantitative application of the results difficult but the qualitative results are informative. This model also neglects the effect of Gausian beam propagation or diffraction which is significant in thick samples, perhaps 100 μm, treated in these papers. Our samples are all less than than 3.25 μm total physical thickness and these last two effects are therefore negligible.

Large Spot

In the plane wave limit, for a laser spot diameter larger than the spacer thickness, Wherrett et al find that the change in temperature is proportional to the total absorbed flux.

$$\Delta T \cong \alpha L I \frac{d_s}{\kappa_s} \qquad 3.18$$

where α is the absorption coefficient

L is the physical thickness of the cavity

I the cavity irradiance

κ_s the substrate thermal conductivity

d_s the spacer thickness

The critical switching irradiance and the critical detuning, below which bistability is unobservable, are found to be

$$I_c \cong \frac{\lambda\alpha\kappa_s}{2\pi(\partial n/\partial T)d_s}\left[\frac{f(R_f,R_b,\alpha d)}{\alpha d}\right] \qquad 3.19$$

and

$$\beta_c = \frac{\sqrt{2}}{4}\sin^{-1}\left[\frac{\sqrt{3(F+2)\ -d}}{2\sqrt{F}}\right]\frac{3(F+2)\ -d}{\sqrt{(F+2)d\ -\ (F+2)^2\ -2F^2}}\ . \qquad 3.20$$

Here:

$$f=\frac{\sqrt{2}}{16}\ \frac{(1-R_\alpha)^2[3(F+2)-d]^2}{(1-R_f)(1+R_b e^{-\alpha d})(1-e^{-\alpha d})\sqrt{[(F+2)d-(F+2)^2-2F^2]}}$$

R_f,R_b are the front and rear stack reflectivities

α is the linear absorption coefficient of the layer

$d=d_s$ the spacer layer thickness

$R_\alpha=\sqrt{R_f R_b}e^{-\alpha d}$ the mean effective reflectivity

$$F = 4R_\alpha/(1-R_\alpha)^2 \qquad 3.21$$

and the finesse $\mathcal{F} = \frac{\pi\sqrt{F}}{2}$.

For a given material there is an optimum αd which minimizes $f/\alpha d$, the cavity factor. Improving the finesse by adding more layers to the spacer will not

reduce the value of the cavity factor f at the minimum because the reduction of L reduces the total absorbed flux .

The frequency dependence of the critical irradiance, I_c, is determined from $\alpha(\omega)$ and $n_2(\omega)$. Considering the temperature dependence of the band edge and background thermal-optic coefficient, it is shown that

$$I_c \propto \lambda_v \frac{\alpha_{tail}}{\partial n/\partial T} \cong \lambda_v \frac{\left[\alpha_g e^{[(h\omega/2\pi - E_g)+\alpha_b]}\right]}{\left\{\frac{\partial E_g}{\partial T}\frac{\partial n}{\partial E_g} + \frac{\partial n}{\partial T}\right\}} \qquad 3.22$$

where:

α_b is the background attenuation

and E_g is the energy gap.

This implies that if one works further from the band edge, in the low loss background absorption region, $\alpha_b \cong 10$ cm^{-1}, 100 μm spacer thickness would be optimum for a reflector of period three, consisting of ZnSe and ThF_4. However, this is not a thin film.

To optimize for samples of smaller thickness obtainable through thermal evaporation, one must consider both the material and the cavity. Unfortunately although the precise form of the band edge and it's temperature dependence strongly affect these calculations they are unavailable for thin films. These two considerations yield different conditions. For an optimized cavity the above authors find

$$I_c \propto \frac{2\pi}{h\omega} \quad \text{with} \quad \frac{h\omega}{2\pi} << E_g. \qquad 3.23$$

whereas for a reasonable spacer thickness

$$I_c \propto E_g g_2\left[\frac{h\omega}{2\pi E_g}, \frac{E_T}{E_g}\right] \qquad 3.24$$

The function g_2 describes the shape of the band tail, and E_T is approximately constant.

Thus in the absence of thickness restrictions they conclude that one should work large band gap materials well below the band edge. For thin film etalons small gap materials should be used near the absorption edge.

Small Spot

One can increase the irradiance by minimizing the spot size. In this case transverse heat flow in the plane of the dielectric layers will be more important than heat flow into the substrate, leading to

$$\Delta T \cong \frac{\alpha I r_0^2}{\kappa} \qquad 3.25$$

κ is the film thermal conductivity.

r_0 is the beam radius at the filter.

The resultant critical irradiance is found to be

$$I_c \cong \lambda_v \frac{\kappa}{(\partial n/\partial T) r_0^2} f(R_f, R_b, \alpha d) \qquad 3.26$$

To optimize the cavity for a small spot :

$$\alpha d \cong \frac{2-R_f-R_b}{4} . \qquad 3.27$$

The optimum frequency is obtained by maximizing $\frac{\partial n}{\partial T}$. This implies operation

just below the bandgap of the material.

The use of nonlinear layers in the stack as well as the spacer reduces the irradiance level necessary for bistability but only slightly. This is explained by considering the total absorbed power. The amount of heat generated depends on both the intrinsic absorption of the material and the irradiance level in the layer (see fig.3.5c) . The heating will be greatest in the spacer and the layers immediately adjacent to it.

Minimum Power

For spot size greater than the thickness of the spacer changing the stack does not alter the minimum power drastically, although the optimum value of αd changes. The minimum critical power is found to be

$$P_{cm} \cong \lambda_g \frac{\kappa_s}{\partial n/\partial T} \alpha r_0 \ . \qquad 3.28$$

Operation near the band edge causes increased absorption leading to loss in cavity finesse. The movement of the band edge with temperature can produce increasing absorption and induce thermal runaway. This can result in increasing absorption switching and/or irreversible damage and instabilities. For these reasons thick samples irradiated at mid-gap are preferred when feasible.

Thin films with high absorption offer an alternative to thick low loss spacers. The linear dependence of the substrate conductivity implies that low conductivity substrates or free standing films would have lower heat loss and lower power requirements.

Transverse thermal isolation is required if the minimum power is to be reduced to the μw level.

In this chapter I have reviewed the theory of optical bistability and the optimization of thermally induced change in the refractive index. This theory indicates that small thermally isolated elements in an array 50 mm on a side should be capable of large parallel data throughput at low power levels. The theory also points out the essentially conflicting demands of low power operation and and fan out. For low power operation one requires a significant amount of absorption, while the ability to address several second stage inputs with the output of a single element requires a large transmission.

THERMAL EVAPORATION

There are many different processes used in the manufacture of optical thin films, the choice of which depends on the nature and the complexity of the design. Chemical vapor deposition (CVD), plasma assisted CVD, sputtering, ion plating, physical vapor deposition (PVD), reactive PVD, or ion assisted PVD are a few of the most prominent. Each of these processes has applications. The most common method, for the manufacture of optical thin films, and the one used exclusively for this work, is PVD.

A description of the process aids in the understanding of the variations observed in the behavior of optical thin films. Real thin films are not the isotropic flat slabs assumed for mathematical convenience in the second chapter. There is significant variation in the optical properties between thin films and bulk material. Theoretical and experimental investigations into the effects of microstructure in thin films is the basis of a great deal of current research. For our purposes a macroscopic description based on a mixed bag of thermodynamic and particle arguments will suffice.

Physical Vapor Deposition is understood by analogy to process by which boiling water evaporates and condenses on the windows in ones kitchen. The process consists of three steps: (I) evaporation of the material from the source; (II) transport of the evaporated material from the source to the substrate; (III) condensation of the vapor stream into a stable film.

The model commonly used is overly simplified in many respects, primarily in the treatment of molecular compounds as simple hard spheres. It is a reasonable model for simple metals. Nonetheless, it incorporates the basic mechanisms by which the processes occur, while remaining tractable. Decomposition and free radical dynamics, in fact all electronic interactions, although present are beyond the scope of this description.

The interested reader is directed to Maissel and Glang (1969), Chopra (1970), or to a review article by Venables, Spiller, and Hunbucken (1985), for a much more complete treatment of this subject .

The Evaporation Process

Overall the process of vacuum deposition of material is clearly not an equilibrium process. There is a net transport of material from the source to the substrate. The pertinent aspects outlined above can be treated as local equilibria; (1) between the solid (if the material sublimes) or liquid and the gaseous phases at the surface of the source, (2) in the vapor stream and (3) between the vapor and the condensate at the substrate.

The Solid-Vapor Transition

Under the assumptions of local equilibrium a material can be characterized by a vapor pressure, β. The condensed phase (solid or liquid), subscript c, and the gaseous phase, subscript g, obey the relations

$$\beta_g = \beta_c \tag{4.1}$$

and

$$d\beta_g = d\beta_c \tag{4.2}$$

The total differential free energy can be used to find the rate of change of β with respect to temperature

$$\frac{d\beta}{dT} = \frac{S_g - S_c}{V_g - V_c} . \tag{4.3}$$

Here S is the entropy and V the volume of the respective phases. These quantities are related to the enthalpy, H, through the Gibbs free energy. From which one arrives at the Clausius-Clapeyron equation

$$\frac{d\beta}{dT} = \frac{H_g - H_c}{T(V_g - V_c)} . \tag{4.4}$$

If one now assumes that the volume of the condensed phase is negligible in relation to that of the vapor and that the gas can be described with the ideal gas law, then

$$V_g - V_c \cong \frac{RT}{\beta} \tag{4.5}$$

and

$$\frac{d\beta}{\beta} = \frac{(H_g - H_c)dT}{RT^2} . \tag{4.6}$$

Where R is Rydbergs constant.

At temperatures above 300k the enthalpy can be approximated by

$$\Delta H = \frac{\Delta H'}{RT} + aT + bT^2 + \frac{c}{T} \tag{4.7}$$

where $\Delta H = H_g - H_c$, while, a, b, c, and $\Delta H'$ are experimentally determined numerical factors characteristic of a given material.

Integration of 4.7 yields

$$\ln\beta = -\frac{\Delta H'}{RT} + \frac{a\ln T}{R} + \frac{bT}{R} + \frac{c}{2RT} + I \ . \qquad 4.8$$

I is a material dependent constant of integration .

Thus one can calculate the temperature necessary for evaporation from standard thermodynamic data and the residual gas pressure. As a rule of thumb one assumes a partial pressure of 10^{-2} mbar as being sufficient to yield an adequate deposition rate.

Transport

The model employed for the vapor stream is that of a swarm of negligibly small particles whose only interaction are elastic collisions. The particles of mass m_i have uniformly random distribution (no preferred direction) and undergo a sufficiently large number of collisions such that the pressure, p, is defined as

$$p_i = \frac{N}{3V} m_i < c_i^2 > \qquad 4.9$$

Where: $\frac{N}{V}$ is the particle density

m_i is the particle mass

$< c^2 > = < v_x^2 + v_y^2 + v_z^2 >$ is the mean square velocity

and <..> implies a continuous average.

This model yields the well known Maxwell-Boltzman velocity distribution. (Adkins, 1982) In the x-direction it can be written as :

$$F(v_{ix}) = \sqrt{\frac{m_i}{2\pi kT}}\, e^{[(m_i v_{ix}/2kT)]}, \qquad 4.10$$

implying that the mean square velocity per particle :

$$\langle c_i^2 \rangle = \frac{8kT}{\pi m_i} \qquad 4.11$$

and the RMS velocity is then

$$\sqrt{\langle c_i^2 \rangle} = 157.94 \sqrt{\frac{T}{m_i}} \quad \text{M/sec.} \qquad 4.12$$

Finally, the mean free path in the vapor stream is found to be

$$\lambda = \frac{kT}{\sqrt{2}\pi\sigma^2 p}. \qquad 4.13$$

where:

k is the Boltzmann constant.

σ is the effective collision cross section.

T is the absolute temperature.

p is the pressure in mbar.

m_i is the molecular weight.

Typical values for mean free path are on the order of meters at a pressure of 10^{-6} mbar.

Film Growth

The process of vapor condensation and film formation directly affect the properties of a thin film. The above relations allow one to calculate the the rate, and the energy distribution of particles incident on a substrate surface. Film growth kinetics are determined by these parameters and those of the substrate. This stage is generally considered as consisting of three substages: condensation; nucleation; and growth.

In the condensation phase, a particle arrives at the surface of the substrate, which is a different material. The impinging atom can then either land on the surface or be reflected. Except for very light or energetic atoms, nearly all incident particles will land. They are then termed adatoms as they are adsorbed onto the surface. In the majority of these adatoms the excess kinetic energy is lost immediately and they are thermalized. The characteristic time for this loss is on the order of the period of a lattice vibration. These particles are only weakly bound. The lack of strong bonding implies mobility. This mobility permits the adatoms to 'run around' on the surface until they are either reemitted or find a niche of slightly lower potential energy where they become localized.

After a sufficient density of adatom monomers is reached on the surface the likelihood of collisions between adatoms becomes significant. At this point the second phase begins. Nucleation is the process whereby the free energy of the surface particles is reduced through the exchange of kinetic for potential energy. The potential energy appears as surface tension. The particles form dimers,

trimers, etc. and so on which are energetically preferred. These stable groups are referred to as nucleation sites. Any newly arriving adatom will now either be adsorbed into the existing nucleation sites, if it condenses near an existing structure or begin the formation of a new site. Eventually the surface of the substrate becomes covered with these nucleation sites, such that any adatom falls within the capture radius, and is absorbed into an existing site. The film exhibits 'islands' of the incoming species surround by a 'sea' of substrate.

These islands continue to grow in both the lateral and vertical directions with the exact structure determined by the particular system under study. The islands then contact and coalesce until arriving adatoms no longer see the substrate and growth ensues. In most cases this growth exhibits a columnar structure which is visible through an electron microscope. This columnar structure appears to be independent of scale, persisting through films of mm thickness where it can be seen with the unaided eye. Columnar growth is a direct result of the nucleation process and yields crystal structure and film properties that are different from those of the bulk material.

The Effects of Structure

The columnar structure discussed in the preceding section has been observed directly and indirectly by many authors (C.C.Lee., F.V.Horowitz, K.H. Guenther, H.A. Macleod, I.J. Hodgkinson). Direct observations by Pulker, Thelen and Guenther(1976), or Macleod(1977) using electron microscopy is very convincing. Indirect evidence comes though the observation of the mechanical,

electrical and optical properties of thin films.

An important parameter in assessing the microstructure of a thin film is the "packing density", P, (Pulker, 1971). Defined as:

$$P = \frac{\text{volume of solid part of film}}{\text{total volume of film}} \qquad 4.14$$

Generally the packing density of a film ranges from 0.7 to 1.0, with most useful materials in the range of 0.85 - 0.95. Packing density has been shown (S.Ogura) to be sensitive to many deposition parameters. It is strongly affected by the residual gas pressure, the deposition rate, and the temperature of the substrate. A packing density less than unity reduces the refractive index of the material. This is because the material is less dense than the bulk .

Low packing density and it's associated disorder can also be responsible for increased absorption in thin films. The voids cause an inhomogeneous broadening and an exponential extension (Urbach tail) of the band edge toward lower energies. The change in the band edge is given by (Weinberger 1984) :

$$\Delta E(h\nu) = \frac{\hbar^2\lambda^2 e^2 \chi^2}{96\pi^2\mu} \; . \qquad 4.15$$

where : $$\frac{1}{\mu} = \frac{1}{m_e^*} + \frac{1}{m_h^*} \qquad 4.16$$

m_e^* , m_h^* are the electron and hole effective masses

λ is the logarithmic slope of the absorption coefficient

$$\alpha = e^{-\lambda[E_g - h\nu]} . \qquad 4.17$$

The void model explains two effects seen in thin films, the reduction in the

refractive index and the change in the response of the absorption coefficient. Another effect that concerns to both the user and manufacturer of thin films is drift. Drift occurs on two different time scales. There is the immediate change in optical properties when a filter is removed from vacuum and there is the long term drift and degradation as the filter ages. These effects are attributed to the columnar structure. The immediate drift of the filter peak wavelength is caused by adsorption of moist air into the previously evacuated voids. As the index of water is roughly thirty percent greater than vacuum this results in an effectively greater film index and thus a shift in the optical properties toward the red. Lee (1984) showed that moisture penetration results from water penetrating first in a direction perpendicular to the layers and then migrating outward. Hodgkinson (1986) indicates that moisture penetration patches are in general of elliptical cross section with the aspect ratio being determined by the obliquity of the columns. The long term drift of the filter can be attributed to changes in the relative humidity and chemical reactions of the absorbed water with the material of the film. Deterioration, cracking and delamination of a coating can be linked to the shielding of short range forces in the film by water. These short range forces counteract the strain in the film and thereby hold it together. Thus moisture can weaken the film substrate interaction by bond transfer, which reduces the work of adhesion. The strain inherent in a film then supplies the work necessary for delamination.

Uniformity of Deposition

Another aspect of the manufacture of interference filters is the uniformity that is achievable. This is a direct result of flux distribution in a coating chamber. This distribution determines the variation of the optical performance that can be expected across a filter.

We consider a point source whose differential mass (dM) distribution into a solid angle $d\omega$ is uniform:

$$dM = \frac{m d\omega}{4\pi}. \qquad 4.18$$

A directed source that consists of: an isothermal enclosure with infinitely thin walls; and a vanishingly small aperture of area dA. This area is small enough that the particles within the enclosure are in thermal equilibrium with the escaping material. Since $\frac{d\omega}{4\pi}$ of the particles are moving toward dA, the number of particles within striking distance of the hole is

$$dN(\phi) = \frac{c \cos\phi \; dt \; dA}{V}. \qquad 4.19$$

After integrating over all velocities the number density is

$$dN(\phi) = \frac{N}{4\pi V}\langle c\rangle \cos\phi \; dA \; dt \; d\omega \quad . \qquad 4.20$$

For identical particles the mass in a differential volume is linearly related to the number of particles

$$dM(\phi) = m d^3N(\phi). \qquad 4.21$$

Identifying

$$\frac{N\langle c\rangle}{4V} = \Gamma \, , \qquad 4.22$$

one obtains

$$dM(\phi) = \frac{\Gamma\, dA\, dt\, d\omega\, \cos\phi}{\pi} . \qquad 4.23$$

The mass deposited is

$$dM(\phi) = \frac{m\, \cos\phi\, d\omega}{\pi} . \qquad 4.24$$

Equation 4.24 is equivalent to Lambert's law, which relates the radiance of a black body to the irradiance on an observation plane.

The substrate is a distance r from the source the amount of material impinging on a surface area dS, whose normal forms an angle θ with respect to the vapor stream (figure 4.1) is: for a point source;

$$dM = \frac{m d\omega}{4\pi} \frac{\cos\theta}{r^2} dS ; \qquad 4.25$$

and, a directed surface source,

$$dM = \frac{m\, \cos\phi\, \cos\theta\, d\omega}{\pi r^2} . \qquad 4.26$$

If the density of the film is ν, then the thickness, t, for a point source is

$$t = \frac{m d\omega}{4\pi} \frac{\cos\theta}{\nu r^2} dS. \qquad 4.27$$

From a directed surface source, the thickness is

$$t = \frac{(m\, \cos\phi\, \cos\theta) d\omega}{\pi \nu r^2} . \qquad 4.28$$

These equations were essentially derived by Holland and Steckelmacher (1952).

As our experiment was performed using a flat plate it is possible to compare the predicted variation in thickness with that actually observed. Since the angles θ and ϕ are equal, equation 4.25 above can be written as

$$t = \frac{mh}{4\pi\nu(h^2+\rho^2)} \qquad 4.29$$

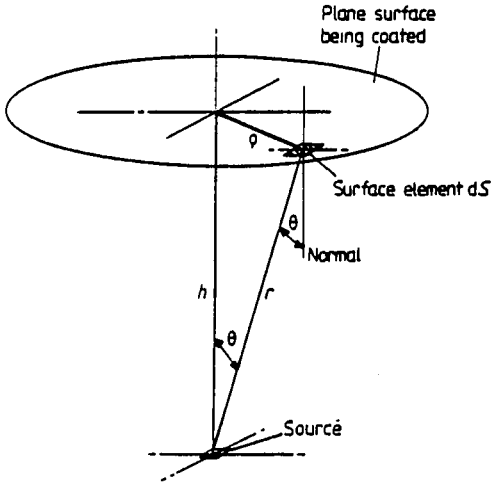

Figure 4.1 *The source-substrate configuration for a flat plate substrate.* (Macleod,1986)

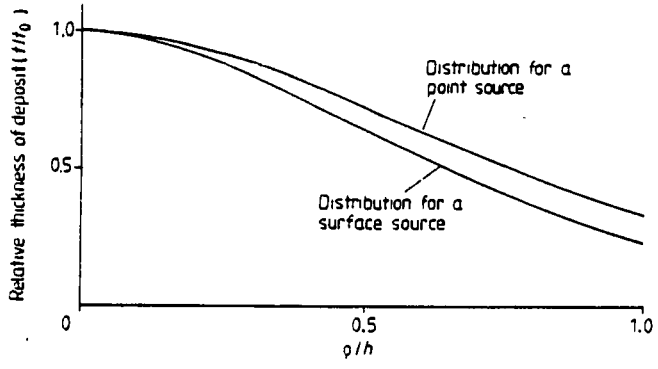

Figure 4.2 *The thickness distribution calculated for a point source and a directed surface source* (Macleod,1986)

and equation 4.28 becomes

$$t=\frac{mh^2}{\pi\nu(h^2+\rho^2)^2} \quad . \qquad 4.30$$

Where figure 4.1 illustrates the configuration: h is the vertical separation of the source and substrate; and ρ is the radial coordinate in the substrate plane.

As can be seen from figure 4.2 this is not a very uniform thickness distribution. To improve the uniformity substrates are usually rotated during deposition. This rotation has the effect of averaging the thickness by averaging the source substrate distance. Consider a directed surface source and a ring of radius ρ on the substrate holder. A point on this ring can be specified by an angle η, in the plane of rotation. The thickness at this point, for a source displaced by a distance R from the center of rotation is

$$t = \frac{mh^2}{\pi\nu(h^2+\rho^2+R^2-2R\rho\cos\ \eta)^2} \ ; \qquad 4.31$$

where r, the distance from the source to the point is given by

$$r^2= (h^2+\rho^2+R^2-2R\rho\cos\ \eta)^2. \qquad 32$$

Thus the mean around the circular path is

$$\langle t\rangle = \frac{m}{\pi\nu}\ \frac{1}{2\pi}\ \frac{h^2 d\eta}{(h^2+\rho^2+R^2-2R\rho\cos\ \eta)^2} \ , \qquad 4.33$$

which by contour integration yields a final thickness distribution

$$t= \frac{m}{\pi\nu}\ \frac{h^2}{(h^2+\rho^2+R^2)^2}\ \frac{1}{\left[1-\frac{2\rho R}{[h^2+\rho^2+R^2]^2}\right]^{3/2}} \ . \qquad 4.34$$

This is an adequate description of the vapor distribution for most thermal sources. The distribution is illustrated in figure 4.3 for several source-substrate arrangements. Normally when calculating the anticipated distribution of a particular plant a directed surface source is assumed. The sources are placed

such that the calculated ideal distribution is obtained. Trial and error corrections can then be made for the best achievable distribution. Once the best position is found care should be taken to insure the sources are always in the correct position and angular orientation.

In cases where even greater uniformity is required one usually uses a rotating domed substrate holder. A domed substrate holder is selected such that the radius of the dome compensates for the radial falloff of the evaporant flux. The greatest uniformity can be obtained through the use of planetary rotation. In a planetary system the substrate has both rotation and revolution. The substrate thus describes a helix, further increasing the averaging introduced by rotation.

Masks are another way to improve the spatial uniformity of the vapor flux. The simplest masks are placed just in front of the substrates so as to correct the radial distribution of the vapor flux. A more recent method developed by Ramsay, Netterfield, and Mugridge is the rotating mask. This method is particularly convenient for large substrates where one is limited to the curvature of the surface and simple rotation. They place a high speed rotating mask between a centrally located source and a rotating substrate achieving a uniformity of 0.1% over a 200 mm substrate.

Thickness Monitoring

In the production of thin film structures the control thickness is essential. Any physical property of a film which varies as a function of thickness can be used for control. The most common methods for thickness monitoring and control

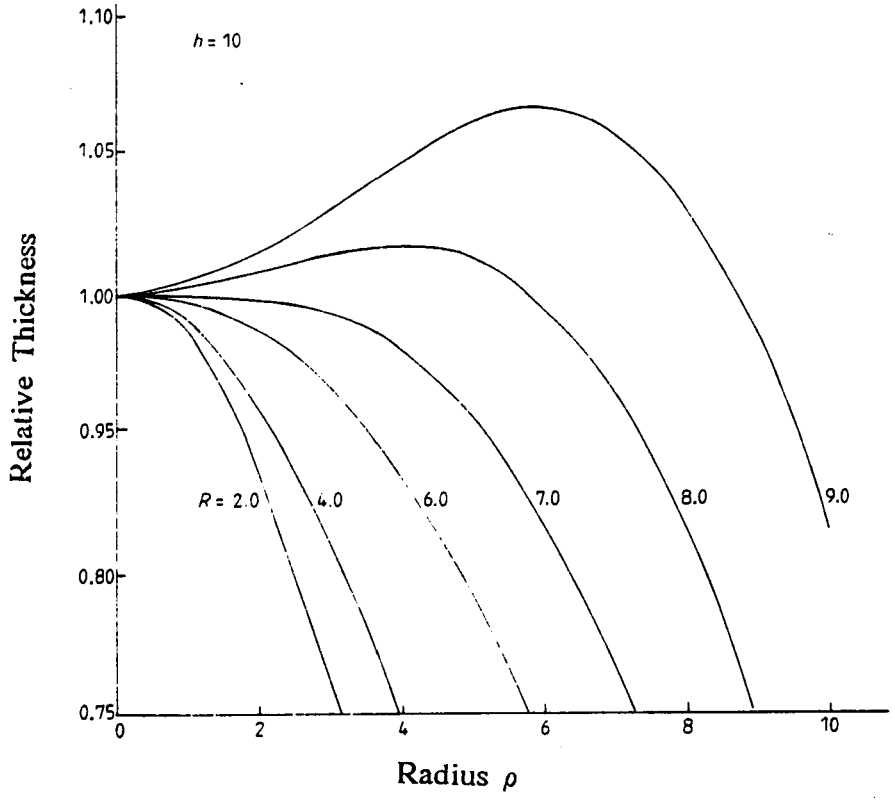

Figure 4.3 *The radial distribution of material for a rotating flat plate for various radial source distances* (Macleod,1986)

are the optical monitor and the quartz crystal microbalance.

Optical Monitor

Optical monitoring is illustrated in figure 4.4. This technique measures the optical properties, either reflection or transmission, of the growing film. The most rudimentary optical monitor is the eye. By observing the color of the light reflected from a substrate one can roughly determine the optical properties. This technique is adequate for simple single layer Antireflection coatings if the specifications are loose. A minimal optical monitor consists of a light source illuminating a test substrate, a wavelength selecting element and a detector. Alternatively, a monochromatic source and a detector can be used. The wavelength selecting element, however, has the added benefit of reducing stray light. The test substrate is either one of the samples (direct monitoring) or a separate monitor chip (indirect). In this work all samples are monitored directly.

Generally the input beam is modulated and the signal is synchronously detected so that background noise, arising from room light or the evaporation source can be reduced with electronic filtering. The wavelength selecting element can be either a narrow band filter, or a spectrally dispersing element, such as a grating or a prism. NBFs are the easiest to employ but care must be taken to eliminate the long wavelength sidebands as thermal evaporation sources have considerable radiant flux in the near infrared. This flux can saturate the detector causing the turning points to be masked. One should also consider the spectral bandwidth of this element as it determines the precision with which any

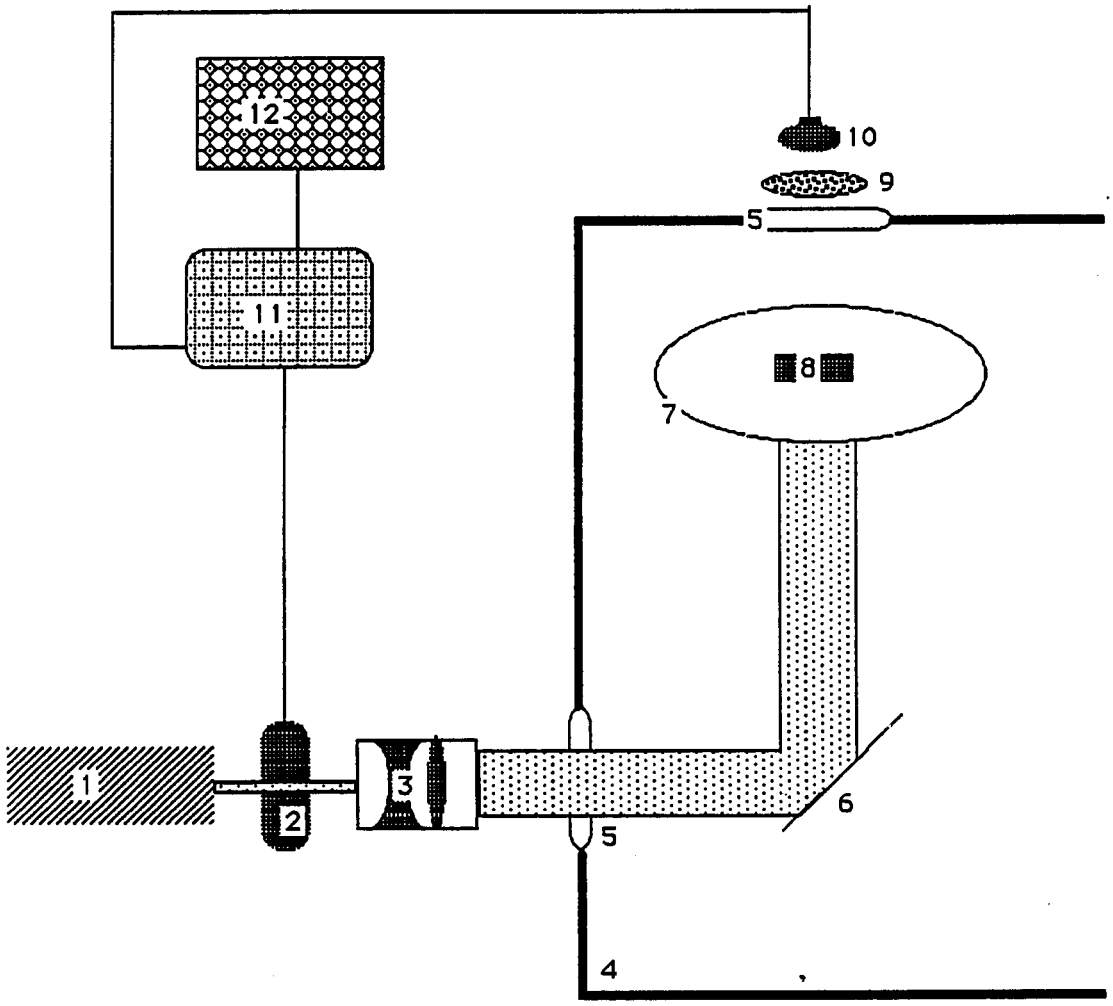

(1) air cooled Ar^+ion laser (λ=5145Å); (2) Beam Chopper; (3) beam expander; (4) vacuum chamber wall; (5) system window; (6) folding mirror (7) substrate holder;(8) substrate; (9) 5145Å Filter; (10) Si Pin detector; (11) Lock-in Amplifier; (12) Strip chart recorder.

Figure 4.4 *Optical monitoring system employed in the Edwards Box coater*

subsequent design can be manufactured. Spectrally dispersive elements, although more complex, lend considerable versatility to the monitoring system(Vidal, Fornier, Pelletier, 1979; Van Milligen et al, 1985). In particular they provide the ability to scan in wavelength. This versatility is not always necessary for simple quarterwave reflectors or NBfs but is required for more rigorous designs such as broadband high reflectance or antireflection coatings.

The evaporation of the layer is terminated, either at turning points (where the structure has a local maximum or minimum) or a predetermined value of the reflectance or transmittance. At the turning points the multilayer is an integral number of quarterwaves optical thickness. This sort of monitoring is preferred for the manufacture of narrow band filters because calibration of the optical system is not required, and optical monitoring systems suffer from drift due to spurious deposition on the windows of the coating chamber. Although one might think that these extrema would be easy to detect, control of thickness is limited to an accuracy on the order of 5 to 10 %. This is due to asymptotic approach of the slope to zero. The operator must predict the turning point by estimating the change in slope and terminate the layer at the appropriate time. 5 % is a large error. Indeed this great of an error in transmittance results from a transmittance error of .5% (Macleod and Ritchmond, 1974; Macleod,1972). This seemingly implies that no workable design could be fabricated.

Any noise in the system further complicates this process. Noise in optical monitors arises from several sources: electronic noise from the detection system; background noise from the evaporation source; and mechanical noise, wobbling of substrate, vignetting of the optical path caused by rotation, and vibration of the plant.

In the case where the design calls for strictly quaterwaves, such as in the production of Fabry-Perot filters there is a great advantage to monitoring either the actual workpiece, or the entire coating on a single monitor chip. This advantage results from the turning point of the layer in question being a function of all the preceding layers (Ritchie, Macleod). Thus if one layer is less than the desired thickness the subsequent layer will not reach it's turning point until its physical thickness is greater than a quarterwave, compensating for the previous error. This error compensation increases the tolerance on absolute error in the determination of the turning point. This compensation changes the effective admittance of the two-layer but the initial error is compensated. This immediate return to the real axis implies that errors due not propagate (Pelletier, 1983) and the method of first order direct monitoring is said to be stable. Error compensation is not present if the layers are monitored on separate chips or if the layers are not quarterwaves. Ritchie has used a Monte-Carlo simulation where random errors were selected from an infinite population of prescribed mean and standard deviation. He finds that the peak transmittance and halfwidth of a filter suffer from errors but that the first order optical monitoring technique is remarkably robust.

Quartz Crystal Monitors

A quartz crystal microbalance measures the mass deposited on an oscillating crystal through the change in resonance frequency. A quartz crystal sliced into thin sections at an angle of 35^0 with respect to the C-X plane 6 is said to be AT

cut. Such a crystal will have a natural resonance which has a minimum dependence on temperature near 30°C. One applies a voltage to the crystal such that it's normal mode of oscillation is a shear mode with the surfaces of the crystals at antinodes. The change in frequency with deposited material is proportional to the amount of material deposited on the crystal, the density and the ratio of acoustic impedances of the material and the quartz crystal. A rather complex dependence on acoustic impedance is one of the major drawbacks to quartz crystal monitoring, as the values of the impedence for many materials of interest is unknown. In thin films the acoustic impedance is a function of the deposition parameters and thickness. The temperature dependence of the oscillating frequency is also a drawback in that it necessitates the inclusion of water cooling and baffling of the sensor head.

Quartz crystals are of great use in automated processes as the signal increases monotonically with thickness, provided one takes the necessary precautions and is willing to make preliminary runs to establish the necessary process parameters. These parameters are the Z-ratio, the tooling factor, and the density. The necessary precautions include: locating the crystal such that it collects a representative sample of the material being deposited at the substrate; having a separate crystal for each material being deposited; and cooling the crystal. Thus quartz crystals are ideally suited to non-quarterwave designs where a large production run justifies the necessary preliminary work. In addition, quartz crystal monitors are well suited for deposition rate control as the change in frequency can be continuously sampled.

The Nuts and Bolts of Evaporation

There are many means of evaporating materials in the high vacuum environment. For use in optical thin film work, the exact choice is dictated by the material to be deposited, the rates desired, the quantity, and the substrate to which the film is applied. Much of the desired information can be found in the standard references (Holland, Chopra) and/or from the catalogs of manufacturers of thin film equipment and materials (Balzers, Cerac, Sloan). The basic types of sources for thermal deposition is presented next.

The first films deposited by a thermal process were Faraday's. He used an "exploding wire" technique. This method is of historical interest, mainly. It consisted of passing a huge current through a thin wire of the material to be evaporated. Kul'gavchuck and Novoskol'tseva (1966) studied the early stages of the explosion process through X-ray techniques but the exact kinematics are not well understood. The effective source temperature is estimated at 10^6 ^{0}K. Thin films formed in this manner tend to show defects due to 'splatter' (the deposition of large clusters).

As vacuum technology has improved, with the subsequent reduction in background pressure, less brutal techniques have developed.

The underlying resistance heating method of Faraday as developed by Nahrwald (1887) is an effective method for many materials. Generally this technique relies on forming a heating element which will support the material to be evaporated. These structures are referred to as "boats" or "canoes" (figure 4.5) depending on their shapes. They are constructed of a refractory metal such as tantalum, molybdenum or tungsten. The particular material being chosen with

regard to the alloying characteristics and vapor pressure of the material to be deposited. In cases where alloying is unavoidable, boats can be covered with alumina, although a penalty is paid in the thermal efficiency. One such material is aluminum. The standard method in our lab is to use a coiled tungsten filament. The aluminum wets the entire surface of the wire and evaporates rapidly avoiding contamination. The drawback is that the filaments become brittle and must be replaced. This is not a major concern in that these filaments are readily fabricated from inexpensive materials.

Resistive heating has intrinsic limitations. The process breaks down if the heating element melts before any appreciable rate is obtained, or burns out due to the presence of reactive gases, which combine with the hot metal. This leads one to consider alternate methods of heating the material. The electron beam source (Holland, Brt. pat. 1951) figure 4.6 is one such alternative. An electron beam source consists of a hot filament electron source (e-beam), an accelerating voltage, and a magnetic focusing field. These elements are arranged such that the electrons travel in an arc of 270^0 before striking a watercooled hearth. The hearth holds the crucible containing the material to be evaporated. In most commercially available designs the bending field is an electromagnet which is ditherred to scan the material being evaporated. The bent path accomplishes two objectives, it reduces the overall size of the device, enabling use in smaller coating plants, and reduces contamination of the filament by the material being evaporated.

The e-beam has several distinct advantages over the resistive heating method. It does not rely on the conductivity of a boat for power delivery. Any convenient material can be used to contain the evaporant, provided it is electrically

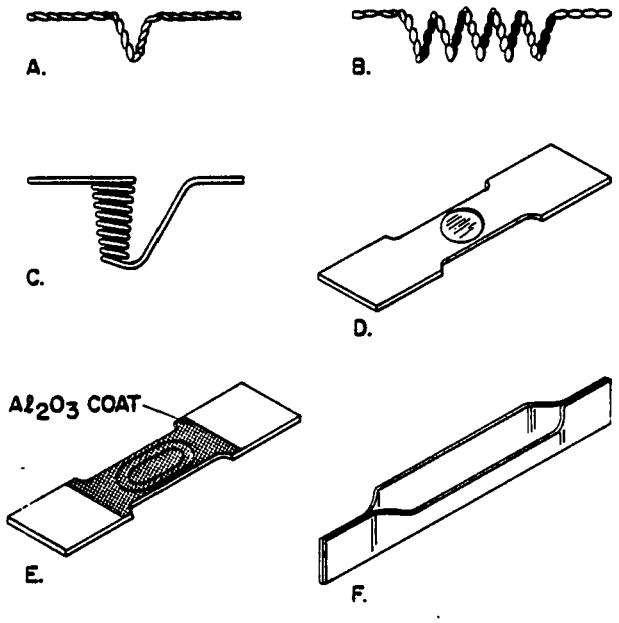

Figure 4.5 *Several common types of resistive sources* used in thin film deposition: (a) Hairpin; (b) coiled filament; (c) coiled basket; (d) dimple; (e) Al_2O_3 coated dimple; (f) canoe.

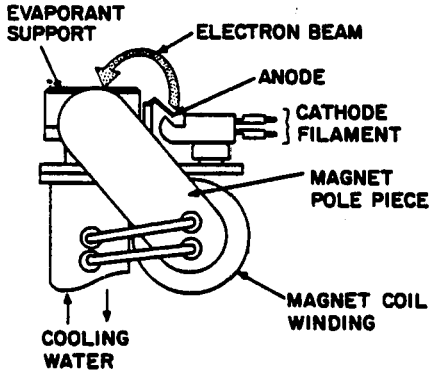

Figure 4.6 *A bent Beam Electron beam source*

conducting. A second advantage is that the power can be delivered to a small area making it possible to evaporate even the most recalcitrant substances. The most difficult materials to evaporate with an e-beam source are those that combine a high melting point with large thermal conductivities and heat capacities, e.g. refractory metals such as molybedenum.

A drawback of electron beam sources is that the flux is not neutral. This leads to difficulty in monitoring thickness with quartz crystals. The presence of ions leads to the accumulation of charge at the sensor which disrupts the driving field and can destroy the crystal. This ion flux can have a beneficial effect in materials that disassociate on evaporation. The presence of ions at the substrate surface increases the rate of reassociation. This improves the packing density of the film.(Macleod,1986)

The plant

The vacuum chamber used in this work is a diffusion pumped box coater custom built by the Edwards corporation in the 1968 for A. F. Turner. The accompanying schematic illustrates the functional parts (figure 4.7).

The pumping system consists of a parallel network of two 6 inch diffusion pumps backed by Sargeant-Welch 1397 mechanical pumps. The diffusion pumps are equipped with a refrigerated baffle to reduce backstreaming of pump oil (dow 7059) into the chamber. The refrigerators are closed circuit compressors with freon-13 as the working fluid. The compressors maintain the optically opaque baffles near -10^0 C. The base vacuum of the plant is

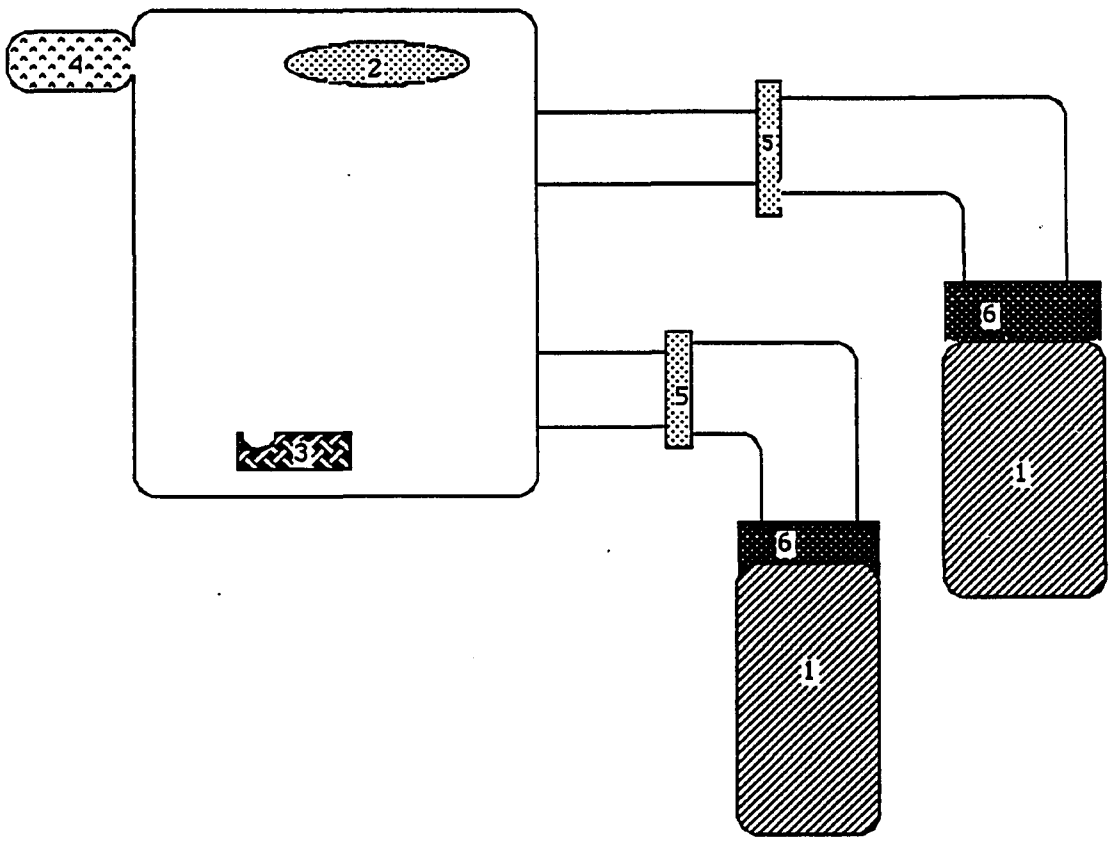

(1) Diffusion Pumps;
(2) Substrates;
(3) Electron Beam Source;
(4) Ionization Pressure Gauge
(5) High Vacuum Valves
(6) Freon Cooled Baffles

Figure 4.8 *A Schematic Representation of the Edwards Box Coater*

approximately 2.6 x 10^{-6} mbar.

The two thermal sources are supplied by a 2 kva step-down transformer with voltage taps of 5, 10, 20, and 40 V. A four pocket, Supersource electron beam source powered by an Airco-Temescal CV-10, 10 kV supply has been used extensively in this work.

The source to substrate distance is about 21" in the vertical and 6", center to center, in the horizontal.

The system is configured for optical or quartz crystal monitoring. The optical monitor uses a small aircooled argon laser as the source , an E G and G model 5205 lockin amplifier, a 514.5 nm filter to reduce the thermal radiation from the source and a UDT pin10D silicon PIN detector. The quartz crystals are controlled with an inficon IC600. The substrate holder is a flat plate. The single substrate is at the center of rotation of the plate and is monitored directly.

EXPERIMENTAL

In the previous chapters the means of constructing narrow band filters and the mathematical description of their linear and nonlinear properties have been presented. In this chapter the experimental test of the model is discussed.

The aim of this experiment is to determine the switching characteristics of a real, as opposed to ideal, NBF by measuring the dependence of the nonlinear behavior on the thickness of the spacer layer. To this end we have selected two materials, commonly used in optical thin films, which have been previously shown to exhibit bistable behavior (Karpushko and Sinitsyn, 1982). We then produced a series of samples in which the spacer layer was held fixed and the reflectivity of the mirrors was varied. It was predicted from computer simulation that a multilayer mirror containing four periods (high/low bi-layers) would yield adequate linear performance. Maintaining the reflectivities "fixed", we then varied the optical thickness of the spacer layer from one to seven halfwaves. After finding that the switching characteristics did not improve markedly for spacers of greater than a full wave, we increased the number of periods in the mirror to five. This did not result in a great decrease in either the linear properties of the filters (halfwidth and transmittance), or the nonlinear characteristics (initial detuning and minimum power).

The standard mirror used in this experiment is a period, p, high-low stack. The design is :

$$\text{glass}|(HL)^p\ mHH\ (LH)^p|\text{glue}|\text{glass}.$$

Where: the glass is Kodak "slide cover glass", a float glass of refractive index, $n \cong 1.518$; $p = 4$ or 5; and $m = 1,2,3,4,6$, or 7. These filters were produced in the Edwards box coater described in the previous chapter. The deposition pressure was typically on the order of 8×10^{-6} mbar. The deposition process typically took 1 hr, at an average deposition rate of 5Å/sec, onto ambient temperature substrates. After allowing the plant to cool in high vacuum for about an hour the samples were removed, and a coverslip cemented over the filter. The coverslip, identical to the substrate, was attached with an ultraviolet curing optical cement, Norland 61. This cementing process retards the long term moisture penetration into the film through the introduction of a physical barrier. After the glue has cured for 24 hours a paper mask with 5 5mm holes is affixed to the front. The holes are arranged as in figure 5.1. The front is the substrate side of the filter. All subsequent measurements are done with the incident radiation striking this interface. This minimizes the flux incident on the optical cement during the switching experiments, reducing the likelihood of damage due to catastrophic failure of the glue. The linear transmission and reflection characteristics of the five sample points are then determined in a Cary 14 spectrophotometer. Figure 5.2 is a typical transmittance measurement. The characteristics of interest in this figure are the variation of peak transmission, peak wavelength, and the full width at half maximum. These quantities reflect the quality of the filter; i.e. the degree of mirror mismatch, amount of loss (scattering and absorption), and the magnitude

of the layer thickness errors.

The samples were than tested for bistability, using the apparatus shown in figure 5.3. To determine the minimum switching power one places the filter to be characterized in the focal plane of the microscope objective on an an x,y,z,θ,ϕ stage. The stage is adjusted such that the point under investigation is at the center of rotation and the light is incident normal to the surface. This minimizes variation in the spot size at the filter as the spot remains in the focal plane as the incident angle is varied. The filter is then rotated away from the normal until a bistable loop is obtained. The power is then reduced and the procedure repeated, until the smallest discernible loop is found. The minimum power is then determined by measuring the average incident power. This procedure is preformed for each of the five areas previously defined. The sampled area is deemed to be "stable" if the hysterises loop remains unchanged for several minutes of operation.

Results and Discussion

The transmittance distribution of the sampling locations is presented in Figure 5.4. In 5.4 (a) is the transmittance distribution of all the data points. In 5.4(b) and 5.4(c) the transmittance distribution of the points for which 'stable' bistability was observed divided according to the two different stacks, p=4 and p=5. It is seen from this figure that a significant fraction of the sampling points showed bistable behavior, but that the transmittance of the filter does not strongly affect the ability to obtain a bistable operation. It does not reveal any information

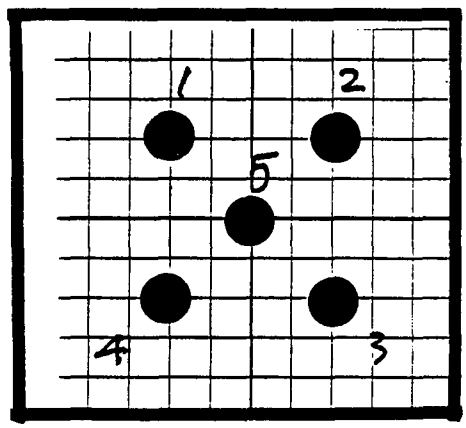

Figure 5.1 *Mask used to determine sampling points*

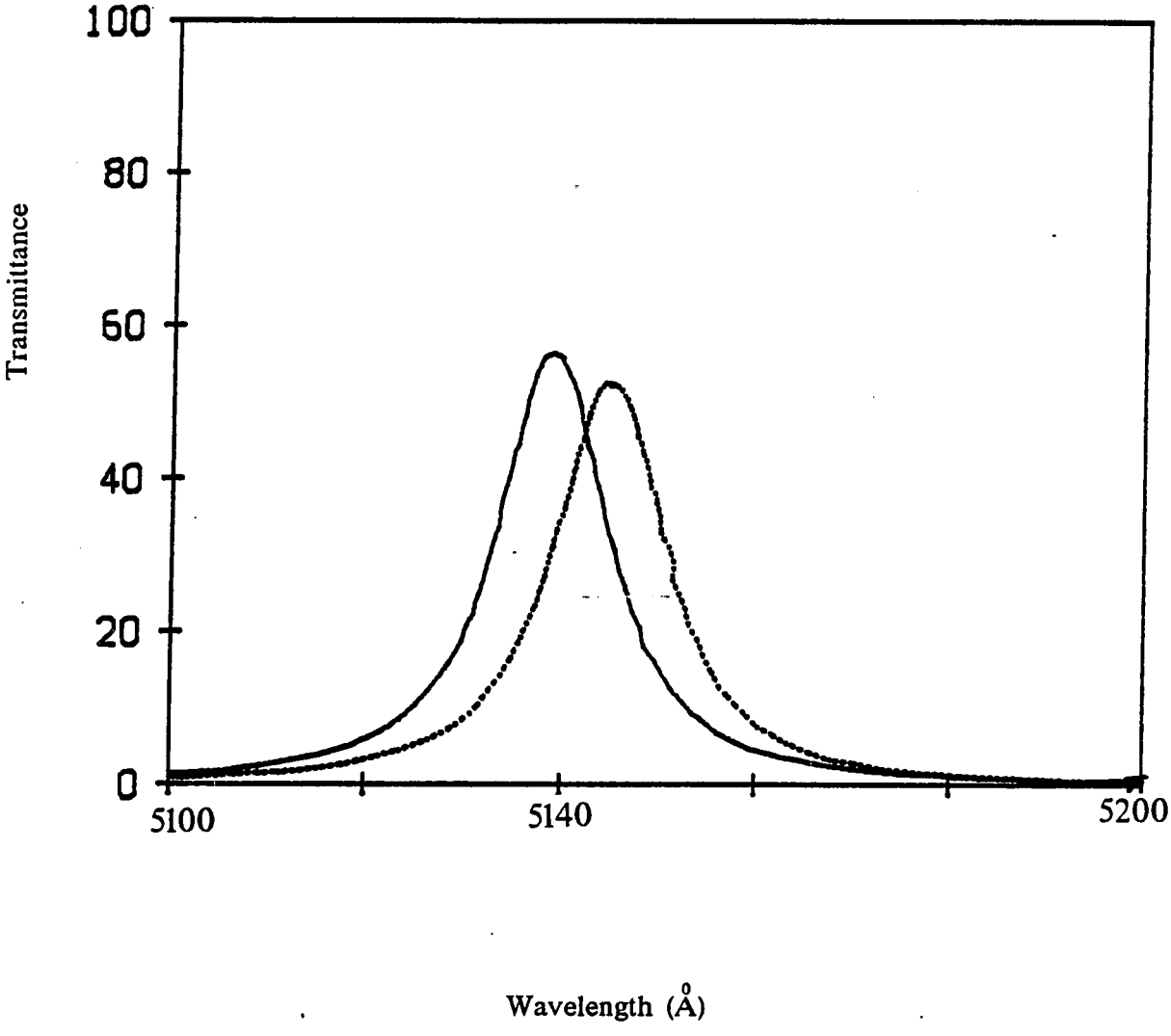

Figure 5.2 *Typical linear performance of a filter* Illustrating the variation in transmittance and halfwidth of the sampled points.

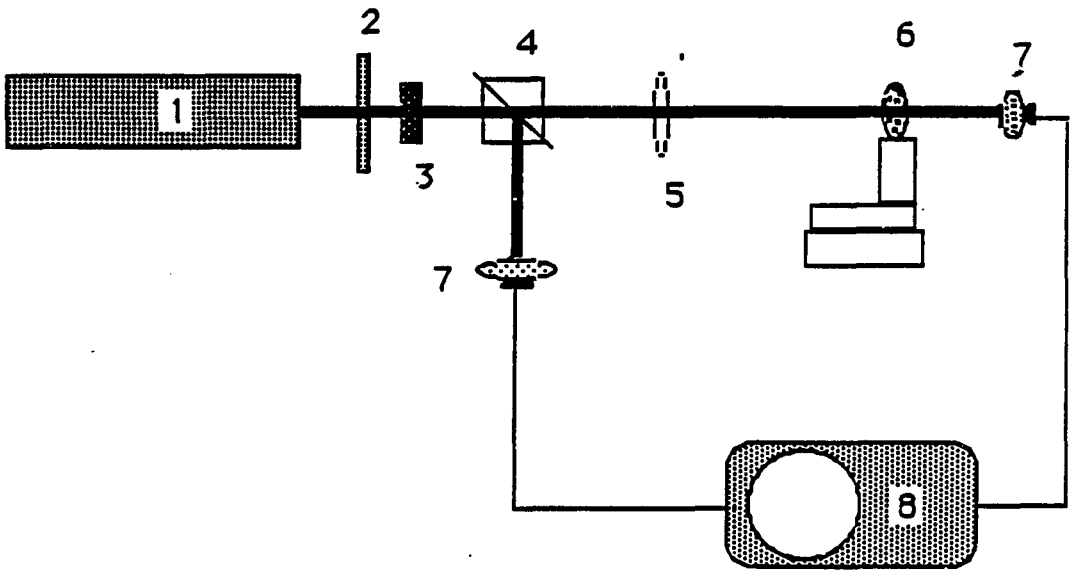

(1) Innova laser;
(2) rotating halfwave plate
(3) linear polarizer at 45°
(4) beam splitter
(5) microscope objective
(6) Sample on X,Y,Z stage
(7) Si detector
(8) oscilloscope .

Figure 5.3 *The experimental apparatus used to determine the nonlinear characteristics of the filters.*

regarding the irradiance level required to obtain bistability. The switching performance should be insensitive to the transmittance of the filter, as the transmittance does not yield information regarding the relative amounts of loss due to reflectance and absorption. Absorption and reflectance losses affect the amount of power required to cause switching. If the reflectance losses are high a larger incident field is required to heat the device enough to cause switching. If absorption is the principle cause of reduction in transmittance then less power is required to switch the device. By comparing the P=4 and p=5 distributions one can ascribe the transmittance loss to reflectance mismatch and/or scatter. The higher period mirrors should have larger fields in the the cavity, and therefore greater loss for identical absorption coefficients. This is not observed. In fact the p=5 filters have a higher average transmittance. The large losses in the p=4 filters must therefore be assigned to mirror mismatch.

In Figure 5.5 the average observed halfwidth of the p=4 filters is compared to that of an ideal filter as a function of the order of the spacer. The halfwidth is seen to improve at first and then level off, eventually falling apart completely. This trend is often seen in the manufacture of optical thin films and can be shown (Ritchie) to result from errors in either the coating process, or to the increase in scattering do to the growth of columns.

The peak transmittance wavelength, do to the inherent error correction in optical monitoring is insensitive to small errors in the thickness of layers other than the spacer. Figure 5.6(a) is a histogram of the peak transmittance wavelength of the filters as sampled in five spots. For random errors in the thickness of the spacer layer, a gausian distribution centered above the optical monitoring wavelength (5145 $\mathring{A}$) is expected. The measured mean is expected to be greater

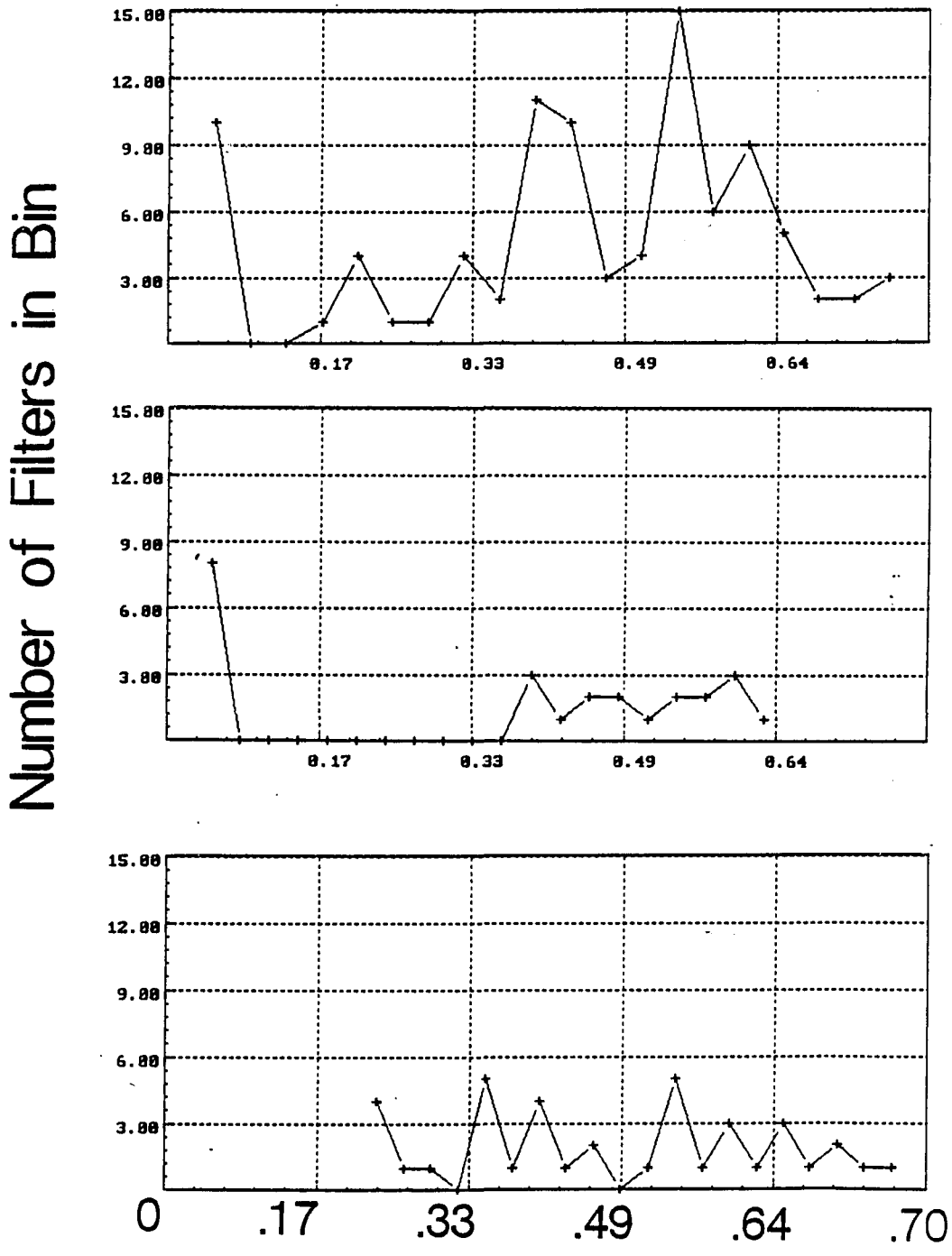

Figure 5.4 *The Transmittance of the sampled locations* is presented in histogram form for: (a) all data, (2) p=4, (3) p = 5.

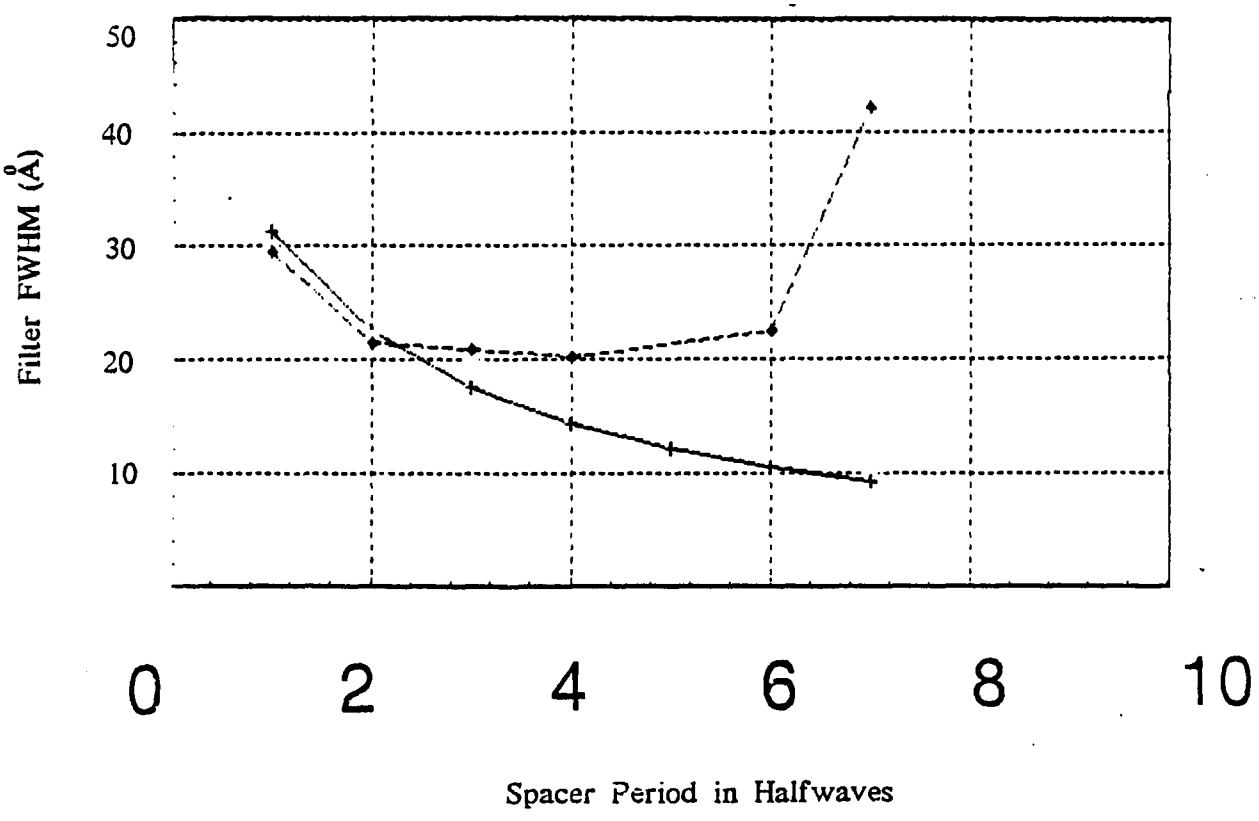

Figure 5.5 *A comparison of the theoretical filter FWHM (solid line) with the experimentally observed halfwidth*

than the monitoring wavelength as the filter shifts to longer wavelengths immediately on venting of the chamber (Saxe, 1985). The mean of the sample distribution is, however, at 5133.6Å, with a Standard deviation of 15.7 Å. This bias is the result of the decrease in layer thickness with radial displacement on the filter. The sampling pattern employed is heavily weighted (4:1) in favor of points away from the center, and consequently of shorter wavelength. In figures 5.6 (b),(c) the peak transmittance of the stable filters for p=4 and 5 are shown. The average is identical for the two groups, but is at a longer wavelength than the total sample. From this we conclude that the observation of bistability in filters with initial peak wavelengths that are much shorter than the laser wavelength is difficult. This is understandable in that if the peak is far from the laser a large temperature change is required to shift the peak into resonance. This implies a large field, which may either, not be available from the source, or be larger than damage threshold of the device. Filters whose linear peak is greater than the laser can be tuned to wavelengths shorter than the laser by tilting to larger angles and thus have observable hysteresis loops.

This brings us to considering the dependence of the switching characteristics of these filters as a function of their linear characteristics. In the chapter on bistability the optimum filter calculations were presented. As noted in that chapter the optical properties of thin films are different from that of the bulk, tabulated data. The errors in the thicknesses of the individual layers which result in the broadening of the transmittance function and reflectivity mismatch can be inferred, but the exact location is unknown. The combination of absorption and mismatch results in the parameter R_α, the effective reflectivity, which can be calculated. It is necessary to make some approximations in

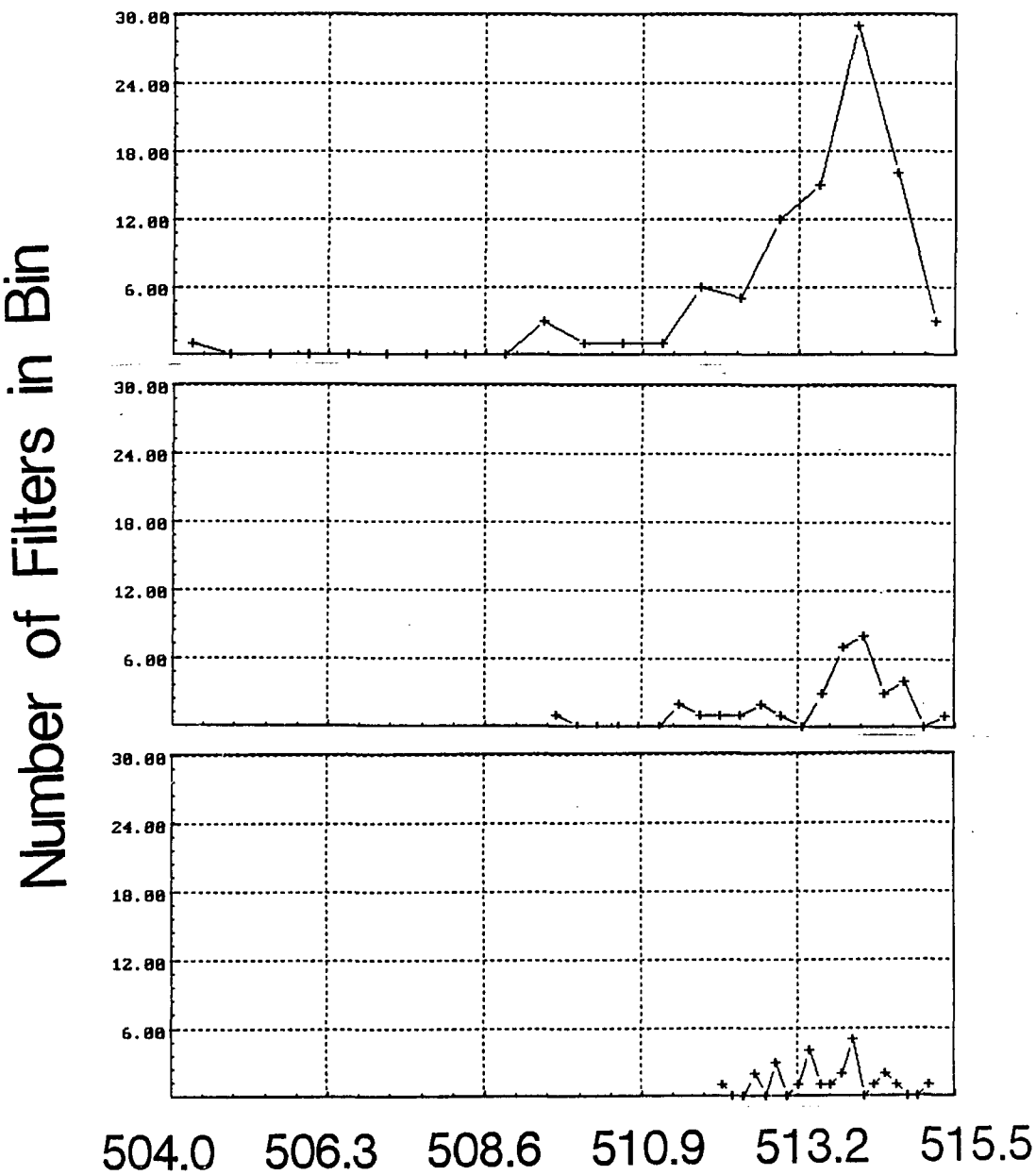

FIgure 5.6 *Histogram of the low power transmittance peak* for: (a) all filters (b) stable filters p=4; (c) stable filters p=5.

predicting the switching characteristics from the linear observations. The major approximation employed in the analysis is that the reflectivity of the two mirrors is essentially identical. With this approximation it is possible to determine the finesse from the observed halfwidth and known spacer order. As the initial critical detuning is determined by the inflection point of the transmittance curve it is only dependent on the finesse. Thus from the measurement of the halfwidth we predict the critical detuning for the sample point. Figure 5.7(a) is the calculated effective wavelength for the locations at which a bistable loop was observed, compared to the filters normal incidence peak. Two regions can be identified, the linear slope region represents the filters whose normal incidence peak was of a shorter wavelength then the critical wavelength. The flat region, with the effective peak wavelength < 5145Å, represents the physical limit due to the positive temperature coefficient of ZnS. In the second figure we have the observed effective peak position, calculated using the linear peak and the observed angular detuning at the minimum. The two curves are similar. In figure 5.7 (c) the data is directly compared. A least squares fit indicates that the slope is .999 with a variance of $3x10^{-3}$. We therefore conclude that the analysis of the switching accurately predicts the minimum detuning necessary for the observation of bistable behavior.

The comparison of the minimum switching power observed to that calculated is somewhat less satisfactory. Figure 5.8 is the absolute minimum switching power obtained for each spacer thickness as compared to the calculated values. The two curves follow the same trend observed for the halfwidth, exhibiting a minimum around a spacer thickness of one wave optical thickness. The experimental curve is also seen to be generally displaced from the calculated

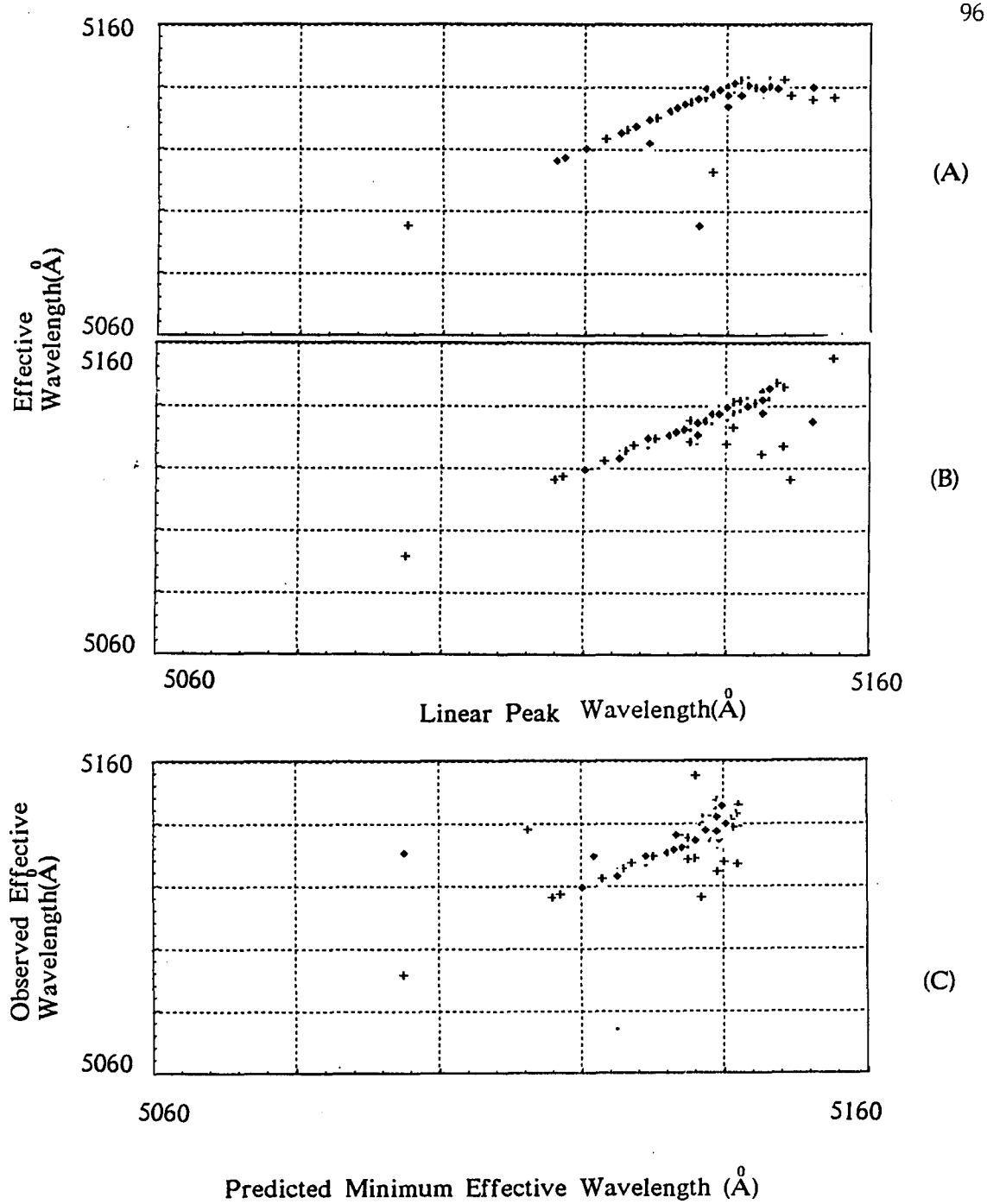

Figure 5.7 *The effective nonlinear peak as a function of the linear peak.* (a) The behavior predicted from the halfwidth and initial wavelength. (b) The observed behavior (c) The observed compared with the predicted.

by approximately a factor of 2. Once again the difference between the p=4 and p=5 stacks is seen to be small.

The experimental uncertainty in the linear and nonlinear measurements are as follows. The Cary Spectrometer is, in the slowest scan mode, accurate to approximately ± 1Å for visible light, and a transmittance accuracy of ± 0.5%. Thus the linear peak wavelength of the filters can be determined to ± 1Å. The determination of the full width at half maximum of the filters is further degraded by the width of the pen. A 1 mm trace corresponds to .6Å, and the resolution of the halfwidth is therefore ± $\sqrt{1.36}$ Å. The measurement of the angle at which bistability is observed is limited to ±1°. This limits the accuracy with which the effective peak of the filter can be determined, for a first order spacer with a detuning in of 3° to ±3Å.

The determination of the argon ion beam radius is also crude, at 50 ±20 Å. The determination of the critical switching power is accurate to ±.17 mW once the sensitivity of the power meter is considered.

Additional discrepancies also arise from using bulk values for the thermal conductivities, refractive indicies and the thermorefractive coefficient.

Conclusion

In this thesis I have attempted to verify the predictions of optimum spacer layer thickness for thermal refractive nonlinear narrow band filters. We have found that the theory accurately predicts the detuning, which depends only on the

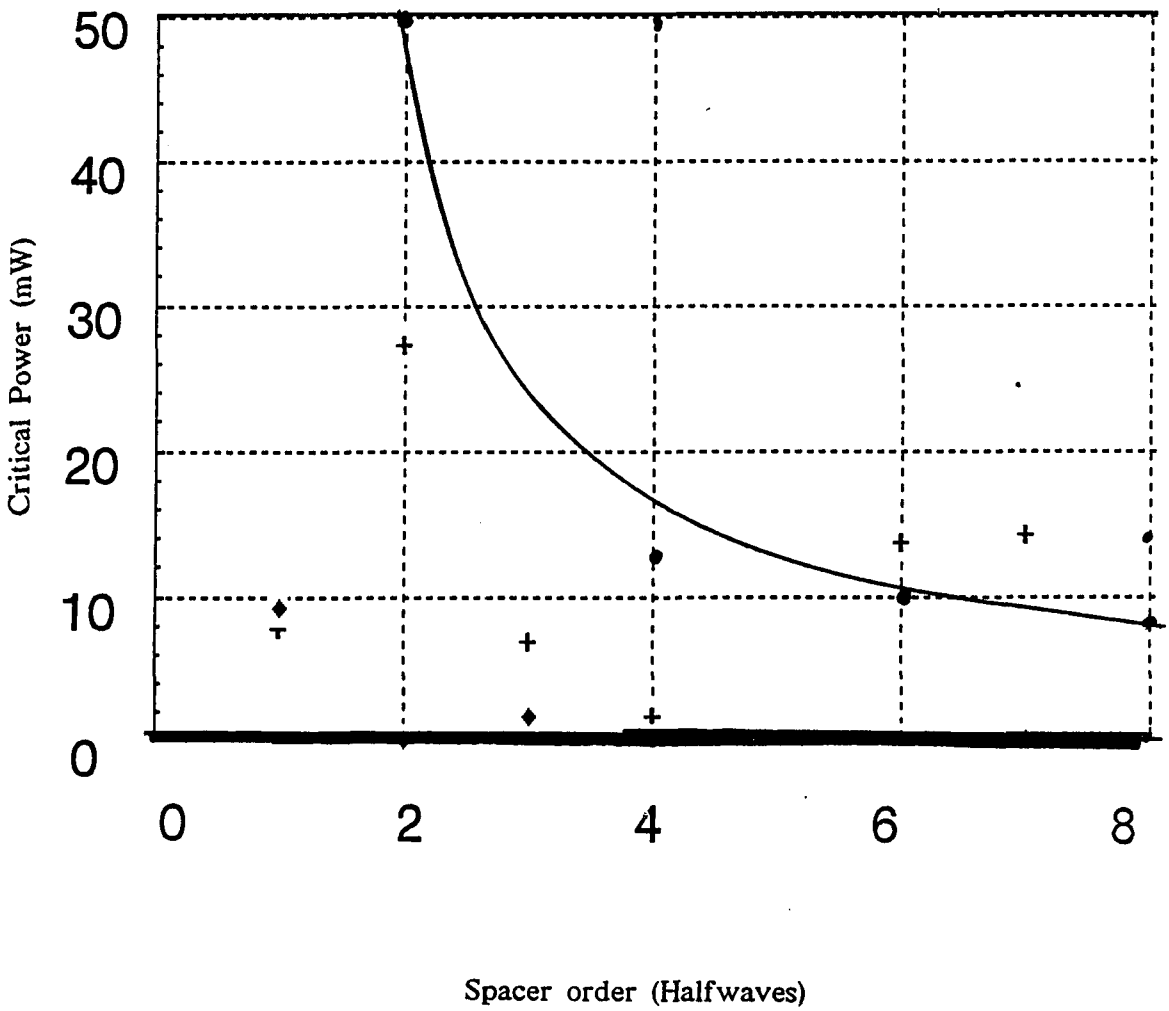

Figure 5.8 *The observed minimum critical power as a function of spacer order.*

shape of the band pass as described by the filters halfwidth. The measurement of the minimum critical power was found to be nearly independent of the spacer thickness, but the precision of the measurements make a quantitative determination difficult. Finally I conclude that extreme caution is necessary in interpreting predictions based on the assumption that a device can be made with an arbitrary degree of accuracy.

REFERENCES

Abeles, F., "Recherches sur la Propagation des ondes Electromagnetiques Sinusoidedales dans les Milieus Stratifies ", Ann. Phys., Paris 12th series, 1950.

Apanasevich, S.P., Karpusko, F.V., and Sinitsyn, G.V., "Response Time of Bistale Devices Based on Evaporated Thin Film Intrferometers", Sov. J. Quantum Electronics 14 (6), 1984.

Atkins, P.W., Physical Chemistry, 2nd ed., W.H. Freeman, 1982.

Baumeister, P., "Optical Coatings: add-ons or Star Performers", Optics News, 12 (6), 1986.

Berning, P.H., Turner, A.F., "Induced Transmission in Absorbing Films Applied to Band Pass Filter Design", Journal of the Optical Society of America 47 (3), 1957.

Born, M. and Wolf, E., Principles of Optics, 6th ed. , Pergamon, 1983.

Chopra, K.L., Thin film Phenomena, McGraw-Hill, 1969.

Dorsel, A., McCullen, J.D., Meystre, P., Vignes, E., Walther, H., "Optical Bistability and Mirror Confinement Induced by Radiation Pressure, " Phys. Rev. Lett. 51 (17), p.1550-1553 , 1981.

Fabry, C. and Perot, A., "Theorie et Applications d'une Nouvelle Methode Spectroscpie Interferentielle", Ann. Chim. Phys., Paris 16 p. 115-144, 1899.

Felber, F.S., Marburger, M.H., "Theory of Nonresonant Multistable Optical Devices", Appl. Phys. Lett., 28 p.731, 1967.

Gibbs, H.M., Optical Bistability: Controlling Light With Light, Academic Press 1985.

Gibbs, H.M., McCall, S.L., Venkatesan, T.N.C., Gossard, A.C., Passner, A., Wiegmann, W., "Optical Bistability in Semiconductors", Appl. Phys. Lett. 35 (16), 1979.

Guenther, K.H., Poulker, H.K., "Electron Microscopical Investigations of Cross Sections of Optical Thin Films", Appl. OPt. 15 p. 2992-7, 1976.

Hecht, E. and Zajac, A., Optics, Addison-Wesley, 1979.

Hemmingway, D.J., Lissberger, P.H., "Properties of Weakly Absorbing Multilayer Systems in Terms of the Concept of Potential Transmittance", Optica Acta 20 (2), 1973.

Herman, J.A., "Bistability in a Thermally-Actvivated Optical Switch", Optics Communications 57 (6), 1986.

Hodgkinson, I.J., Jacobson, M.R., Potoff, R.H., Sikkens, M., Sprague, R., "Water Penetration Fronts in Thin Films Deposited at Oblique Incidence", Thin Solid Films 138, p.286-296, 1986.

Holland, L., Steckelmacher, W. "The Distribution of Thin Films Condensed on Surfaces by the Vacuum Evaporation Method", Vacuum 2 p. 346, 1952.

Holland, L., Vacuum Deposition of Thin Films, Chapman and Hall, 1950.

Horowitz, F., Structure-Induced Optical Anisoprotry in Thin Films, Ph.D. Dissertation, University of Arizona, 1983.

Huang, A., "Parallel Algorithms for Optical Digital Computers", 10th International Optical Computing Conference, IEEE Cat. 83ch1880-4, p. 13, 1983.

Jin, R., Wang, L., Sprague, R.W., Olbright, G.R., Kulcke, H., Gigioli, G., Gibbs, H.M., Macleod, H.A., Peyghambarian, N., "Simultaneous Optical Bistable Switching of Adjacent Pixels on a Uniform ZnS Interference Filter", Optical Bistability III, Conference Proceedings, Springer-Verlag, 1986.

Karpusko, F.V., Sinitsyn, G.V.,"An Optical Logic Element for Integrated Optics in a Nonlinear Semiconductor Interferometer", J. Appl. Spectroscopy (USSR) 29, p. 1328, 1978.

Karpusko, F.V., Sinitsyn, G.V., "Switching of a Laser Emisson Spectrum by an External Optical Signal",Sov. J. Quantum Electronics9,p. 520, 1979.

Karpusko, F.V., Sinitsyn, G.V., "The Anomolous Nonlinearity and Optical Bistability in Thin Film Interference Structures", Appl. Phys. B 28, p. 137, 1982.

Kul'garchuck and Nov'skoe, Sov. Phys. Tech. Phys. 11, p. 406, 1966.

Marburger, J.H., and Felber,F.S., "Theory of Lossless Nonlinear Fabry-Perot Interferometer", Phys. Rev. A 17 p.335, 1978.

McCall, S.L., Gibbs, H.M., Churchill, G.G., Venkatesan, T.N.C., "Optical Transistor and Bistability", Bull. Am. Phys. Soc. 20, p. 636, 1975.

Lee, C.C., Moisture Adsorption and Optical Instability in Thin Film Coatings , Ph.d Dissertation, University of Arizona, 1983.

Lissberger, P.H., "Properties of All-Dielectric Interference Filters, I, A New Method of Calculation", Journal of the Optical Society of America 49 (2), 1959.

Lissberger, P.H., Wilcock, W.L., "Properties of All-Dielectric Interference Filters, II, Filters in Parallel Beams of Light Incident Obliquely and in Convergent Beams", Journal of the Optical Society of America 49 (2), 1959.

Lohman, A., "What Clasical Optics can do for the Digital Optical Computer", Appl. Opt. 25 (10), p. 1543, 1986.

Lorrain, P. and Corson, D., Electromagnetic Fields and Waves , 2nd ed, W.H. Freeman and Co., 1970

Macleod, H.A., "Turning Value Monitoring of Narrow-Band All-Dielectric Thin-Film Optical Filters", Optica Acta 19 (1), p.1-28, 1972.

Macleod, H.A., "Absorption in Turning Value Monitoring of Narrow Band Thin Film Optical Filters", Optica Atca 20 (7), 1973.

Macleod, H.A., "Thin Film Narrow Band Filters", Thin Solid Films 34, p. 335-342, 1976.

Macleod, H.A., "The Monitoring of Thin Films for Optical Purposes", Vacuum 27 (4) p. 383, 1977.

Macleod, H.A.,"A New Approach to the Design of Metal Dielectric Thin Film Optical Coatings", Optica Atca 25 (2), 1978.

Macleod, H.A., Thin Film Optical Filters, 2nd ed. , Macmillan, 1986

Macleod,H.A., and Ritchmond, D., "Turning Value Monitorring of Narrow-Band all Dielectric Thin Film Optical Filters", Optica Acta 19, p. 1-28, 1974.

Maissel, L.I., Glang, R., Handbook of Thin Film Technology , McGraw-Hill, 1970.

Miller, D.A.B, Smith, S.D., Seaton, C.T., "Optical Bistability in Semiconductors", IEEE Journal of Quantum Optics QE-17 (3), 1981.

Miller, D.A.B. , "Refractive Fabry-perot Bistability with Linear Absorbtion: Theory of Operation and Cavity Optimization "IEEE Journal of Quantum Electronics 17 (3), 1981.

Nahrwald, R., Ann. Physik 31, p.467, 1887.

Olbright, G.R., Peyghambarian,N., Gibbs, H.M., Macleod, H.A., Van Milligen, F. "Microsecond Room-Temperature Optical Bistability and Crosstalk Studies in Zns and ZnSe Interference Filters with Visible Light and Milliwatt Powers", Appl. Phys. Lett. 45 (15), 1984.

Ogura, S., Some Features of the Behaviour of Optical Thin Films, Ph.D. Dissertration, Newcastle-upon-Tyne Polytechnic, 1975.

Pidgeon, C.R., Smith, S.D. "Resolving Power of Multilayer Filters In Non-parallel Light", Journal of the Optical Society of America 54 (12), 1964.

Guenther, K.H., Thelen, H.K., "Electron Microscopical Investigations of Cross Sections of Optical Thin Films", Appl. Opt. 15 p.2992-7, 1976.

Pelletier, E., " Monitoring of Optical Thin Films During Deposition", SPIE Vol. 401, Thin Film Phenomena, p.74-82, 1983.

Poulker,H.K. and Jung,E., "Correlation Between Film Structrure and Sorption Behaviour of Vapour Deposited ZnS, Cryolite, and MgF_2 Films", Thin Solid Films 9 p.57-66, 1971.

Polster, H.D. "A Symmetrical All Dielectric Interference Filter", Journal of the Optical Society of America 42 (1), 1952.

Ramsay, J.V., Netterfield, R.P., Mugridge, E.C.V., "Large-Arrea Uniform Evaporated Thin Films", Vacuum 24 p. 337-340, 1974.

Ritchie, F.S. Multilayer Filters for the Infra-red region 10-100 μM, Ph.D. Thesis, University of Reading , England, 1970.

Sahlen, O., "Switching Power dependence on Spot Size in Bistable ZnS Etalons", Optics Communications 59 (3), 1986.

Sargent, M., III, Scully, M.O., Lamb, W.E.Jr., Laser Physics , Addison-Wesley, 1974.

Seidel, H., "Bistable Optical Circuit using Saturable Absorber within a Resonant Cavity", U.S. patent 3,610,731 , filed 1969.

Smith, S.D. , Mathew, J.G.H, Taghizadeh, Walker, A.C., Wherrett, B.S., and Hendry, A., "Room Temperature, Visible Wavelentgh Optical Bistabilty in ZnSe Interference Filters", Optics Communications 51 (5), 1984.

Smith, S.D., "Design of Multilayers by Considering two Effective Interfaces", Journal of the Optical Society of America 48 (1) 1958.

Szöke, A., Daneu, V., Goldhar, J., Kurnit, N.A., "Bistable Optical Element and its Applications", Appl. Phys. Lett. 15, p.376, 1969.

Toyzawa, Y., "Population Instability and Optical Anomalies in High Density Excited Systems", Solid State Communications 32, p. 533, 1978.

Venables, J.A., Spiller, G.D.T., Hanbucken, M., "Nucleation and Growth of Thin Films", Rep. Prog. Phys. 47 p. 399-459, 1984.

Wherrett, B.S., "Fabry-Perot Bistable Cavity Optimization on Reflection", IEEE Journal of Quantum Electronics, **20** (6) , 1984.

Wherrett, B.S., Hutchings, D., Russell, D. "Optical Bistable Interference Filters: Optimization Considerations", J. Opt. Soc. Am. B **3** (2), 1986.

Wienberger, D., Optical Bistability in ZnS and ZnSe Thin Film Interference Filters and in CuCl Etalons, Ph.D dissertation, University of Arizona, 1984.

Van Milligen, F.J., Bovard, B. Jacobson, M.R., Mueller, J., Potoff, R., Shoemaker, R.L., Macleod,H.A., "Development of an Atomated Scanning Monochromator for Monitoring thin films", Appl. OPt. **24** (12),p. 1799, 1985.

Vidal, B., Fornier, A., Pelletier, E., "Wideband Optical Monitoring of Nonquarterwave Multilayer Filters", Appl. Opt. **22** (18), p.3851 ,1979.